THESIS

DESIGN AND FLOW CHARACTERIZATION OF AN INDRAFT SUPERSONIC WIND TUNNEL FOR SCRAMJET TESTING

Submitted by

Spencer J. Teeter

Department of Mechanical Engineering

In partial fulfillment of the requirements

For the Degree of Master of Science

Colorado State University

Fort Collins, Colorado

Fall 2024

Master's Committee:

Advisor: Ciprian Dumitrache

Bret Windom
Thomas Bradley

ABSTRACT

DESIGN AND FLOW CHARACTERIZATION OF AN INDRAFT SUPERSONIC WIND TUNNEL FOR SCRAMJET TESTING

This thesis describes the Colorado State University supersonic wind tunnel design, manufacture, assembly, and validation. The overarching goal of this research is to develop a ground testing platform for studying airbreathing hypersonic propulsion systems. Problems of interest include design of isolators, fuel injection systems, ignition and flame stabilization, shock-boundary layer interaction, and aero-thermo-elastic interactions in scramjet vehicles.

An indraft-type tunnel was chosen for its simplicity, low capital investment, and low power requirement. Its main features are large windows for advanced optical flow diagnostics, modular experimental mounting system, cycle time under 15 minutes, and adjustable size up to 5.25” x 5.25” x 25”. The bulk of this thesis research focuses on flow characterization using a Mach 2.5 nozzle and a test section of 5.25” x 1.57”. To this effect, we determined the Mach number using shockwave schlieren and stagnation pressure measurements over longitudinal and transverse scans in the tunnel test section. Experiments show that steady-state flow consistently develops in 0.5 seconds at a uniform Mach 2.4 at the entrance of the test section decreasing to 1.5 at the exit. Nozzle outflow and shot-to-shot Mach number variation was low, while measurement deviation increased near the test section walls and exit due to boundary layer growth.

By studying phenomena such as fuel mixing, ignition, and flame stability at high Mach numbers inside of a supersonic wind tunnel, research at the CSU’s Aerospace Propulsion and Diagnostics Laboratory seeks to overcome the limitations of current scramjet technologies.

ACKNOWLEDGEMENTS

I am profoundly thankful to my advisor and mentor, Dr. Ciprian Dumitrache, for his unwavering support, boundless passion, and exceptional expertise. His teachings have been instrumental throughout this journey. I extend my gratitude to the Office of the Vice President for Research at Colorado State University for their invaluable support of this project.

I am also grateful to my friends and family for their belief in me. Their encouragement and love have been a constant source of motivation. Lastly, I want to express my appreciation to the many other professors and fellow students at Colorado State University who share my enthusiasm for learning and celebrating each other's success.

DEDICATION

I dedicate this thesis to the Teeter family.

TABLE OF CONTENTS

LIST OF TABLES

LIST OF FIGURES

Chapter 1 Introduction to Hypersonics

1.1 The Dawn of Hypersonic Propulsion

Today, rockets carry their fuel, oxidizer, and a payload into space. This is analogous to hiking with a lunch sack and scuba tank. Sure, carrying some food is a good idea, but carrying air is redundant when you are within Earth's oxygen-rich atmosphere. Why do we use rockets to accelerate the fastest man-made objects? There is no restriction in physics preventing humans from flying from the surface of Earth to space with air-breathing aircraft. The key to developing faster transportation, hypersonic missiles, and spaceplanes is supersonic combustion.

Decades of propulsion research have matured the turbojet and ramjet, while paving a way for the emerging supersonic combusting ramjet, or scramjet. Current power and thrust generation exclusively use subsonic flow to combust fuels and expand the hot fluid to extract useful work. To date, the fastest airbreathing engine that entered mass production was the Pratt & Whitney J58, which equipped the SR-71 Blackbird strategic reconnaissance aircraft [1]. The J58 used a gas turbine-ramjet combined cycle and enabled the SR-71 Blackbird to achieve a vehicle speed near Mach 3.4. This is not a hard limit on the speed of transportation, but rather a scientific and engineering challenge to design power cycles that can operate at hypersonic speed.

Rather intuitively, aircraft engine efficiency generally goes down as flight speed increases. For example, in propeller aircraft, as screw pitch of the prop approaches the speed of the aircraft, system efficiency rapidly drops off as the propeller is now moving faster and creating more drag but is no longer able to create additional thrust. Propulsive efficiency is the ratio of useful power output to the total power output. As aircraft speed increases, the velocity of the exhaust relative to the aircraft must also increase to produce sufficient thrust. A higher exhaust velocity results in a lower

propulsive efficiency; more energy is wasted in accelerating the exhaust gases rather than providing useful thrust, adding momentum to the aircraft. Propellers are so efficient because they move a large amount of air more slowly than a jet engine which accelerates its exhaust stream to a much higher speed, but this is only true up to a point. At transonic speeds, propeller efficiency rapidly drops off due to wave drag. Airfoils at transonic speeds form compressible flow features, ruining aerodynamic performance.

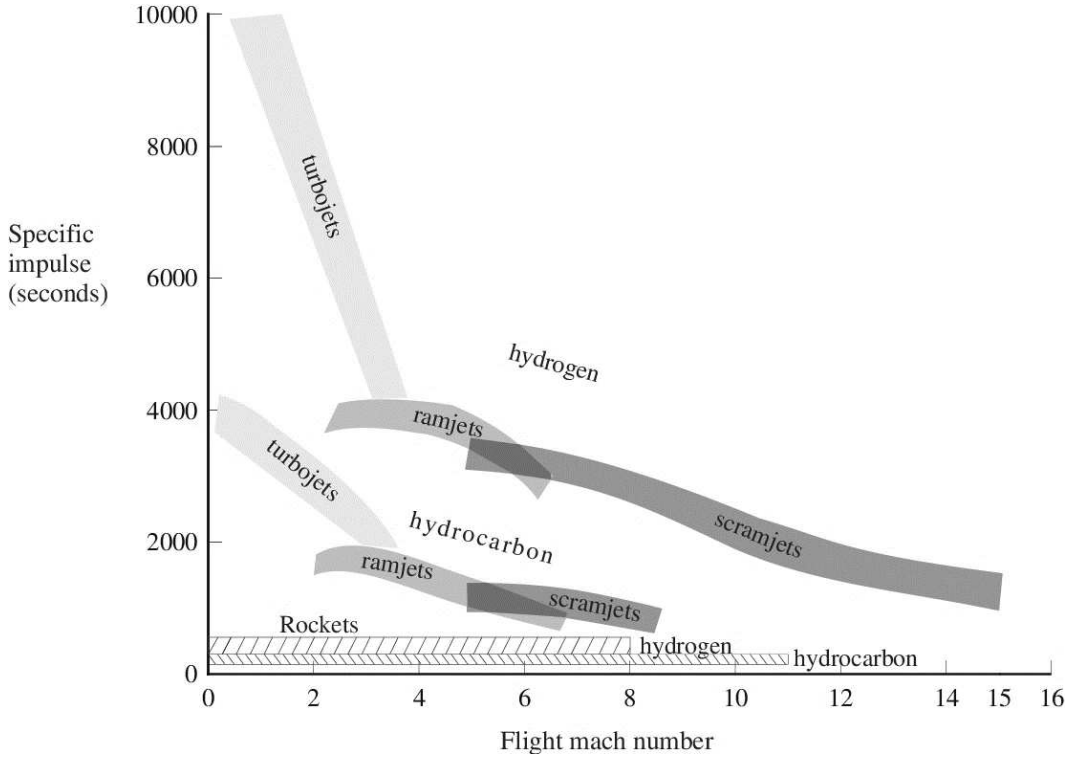

Figure 1.1: Vehicle propulsion alternatives for high-speed flight. For each class of propulsion system both hydrocarbon and hydrogen fueled performance is shown [2].

Turbojets pick up where propellers leave off, having higher efficiency at transonic and supersonic speeds (Figure 1.1). The engine's turbomachinery processes oncoming air through compression, combustion, and expansion (Figure 1.2a). Turbojets are not exposed to supersonic or transonic air directly; they are often proceeded by a supersonic inlet and diffuser which conditions the flow to a lower, subsonic speed. At supersonic speeds, the inlet constitutes the first stage of the

engine's compression process. The turbojet drops off in efficiency around Mach 3 (Figure 1.1), when the temperature after the compressor becomes unreasonably high for the materials of the engine, and combustion can only produce diminishing returns.

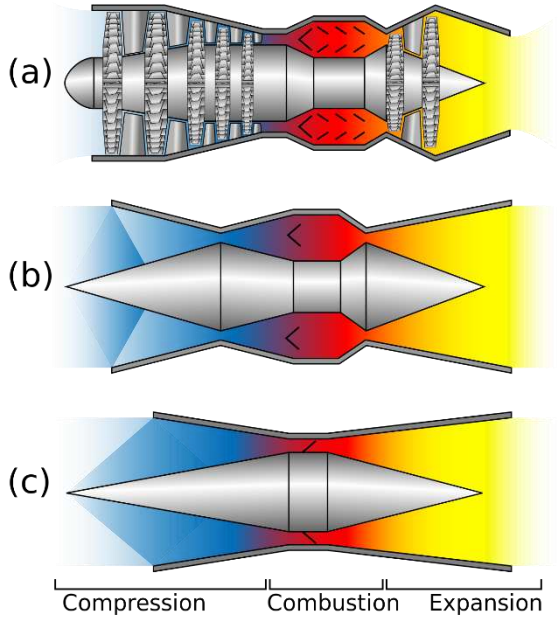

Figure 1.2: (a) Turbojet engine. (b) Ramjet engine. (c) Scramjet engine.

The ramjet is a straightforward, yet highly effective type of air-breathing propulsion system, distinguished by its lack of moving parts (Figure 1.2b). The engine compresses incoming air using the ram effect, which occurs when an aircraft moves forward at high speeds, forcing air into the intake and increasing its pressure and temperature. A series of shock waves within the intake ensures that by the time the air reaches the combustion chamber, it has slowed to subsonic speeds. This is the sole compression process in a ramjet, making it simpler and more efficient than turbojets at high speeds, particularly above Mach 3. In a ramjet, combustion occurs at constant pressure. The incoming air, having been compressed and slowed, mixes with fuel in the combustion chamber, where it is ignited. The resulting hot gases are then expelled through a nozzle, producing thrust. This process is efficient at speeds ranging from Mach 3 to 6 (Figure 1.1), where the cooler

air intake allows for greater heat release from combustion. However, as the aircraft speed increases beyond this range, the air temperature in the ramjet combustor can exceed 2000 K, leading to gas dissociation and reduced combustion efficiency.

Scramjets, or Supersonic Combustion Ramjets, represent the pinnacle of air-breathing propulsion. They build upon the principles of ramjets but extend their operational speed range significantly by utilizing supersonic combustion. Like ramjets, scramjets have no moving parts and rely on an inlet to compress the incoming high-speed air (Figure 1.2c). However, unlike ramjets, scramjets do not decelerate the air to subsonic speeds before combustion. The air remains supersonic as it passes into the combustion chamber. This design decreases the compression ratio, keeping air at a lower temperature than would occur in a subsonic combustion process. The lower air temperature allows for efficient fuel energy extraction, raising the gas temperature without causing excessive combustion product dissociation. The high-temperature gas is then accelerated through a nozzle to produce thrust. This supersonic combustion mechanism enables scramjets to operate efficiently at speeds significantly higher than those achievable by ramjets, extending the practical range of air-breathing propulsion systems to hypersonic velocities (Figure 1.1).

1.2 Hypersonic Research Programs

1.2.1 National Aero-Space Plane (NASP)

Figure 1.3: National Aero-Space Plane 1/3 scale wind tunnel model [3].

The National Aero-Space Plane (NASP), or X-30, was envisioned as a single-stage-to-orbit vehicle capable of taking off and landing on conventional runways. This ambitious project aimed to revolutionize space travel by enabling horizontal takeoff and landing, utilizing air-breathing propulsion for a significant portion of its ascent. The design required a minimum-weight structure that could withstand large temperature variations, leading to inherent flexibilities and susceptibility to stiffness reductions due to thermal loads and gradients. These factors necessitated extensive research into the vehicle's aeroelastic characteristics.

The National Aero-Space Plane project aimed to develop technologies for hypersonic cruise vehicles and single-stage-to-orbit systems with air-breathing propulsion and horizontal take-off and landing. Although funding was cut by Congress in 1994 [4], preventing the construction of a full-scale aircraft that was expected to reach Mach 25, the program made significant

advancements in high-temperature carbon-carbon materials, lightweight titanium and beryllium alloys, and high-strength, corrosion-resistant titanium-alloy composites. These technological developments, along with the work on supersonic-combustion ramjet propulsion, benefits future U.S. aerospace projects in the hypersonic domain.

NASA Langley Research Center and the USAF Wright Laboratory conducted extensive aeroelasticity research to support the NASP design. This research included the development of new computational codes for predicting unsteady aerodynamic pressures, studies on aerodynamic heating effects, and the impact of fuselage flexibility on control system stability [5]. The research aimed to validate computational tools and gain a better understanding of the aeroelastic response of the NASP vehicle. Scale models of the vehicle and its components, such as lifting surfaces and fuselage panels, were tested to obtain data for validating analytical codes. A joint effort by NASA, the Department of Defense, and five major contractors led to the creation of a 1/3-scale concept demonstrator, tested in a high-temperature tunnel between 1986 and 1994. These experiments included testing in various wind tunnels across the Mach number range, providing crucial data for code validation and ensuring the reliability of the computational predictions.

The NASP program, despite not achieving a full-scale flight, made significant advancements in aerospace technology. The research conducted on the NASP's aeroelasticity, thermal effects, and control system stability provided valuable insights and developed technologies for following hypersonic vehicle designs.

1.2.2 HyShot Program

Figure 1.4: HyShot payload [6].

The HyShot program, initiated by the University of Queensland in Australia, aimed to test and validate scramjet engine technology through a series of flight experiments. Launched in 2002, the program utilized sounding rockets to carry the scramjet engines to the required altitudes and speeds, achieving flight conditions necessary for scramjet operation.

Among the key accomplishments was the successful demonstration of supersonic combustion in flight above Mach 7.5 during the HyShot 2 experiment [6]. The data collected confirmed the presence of supersonic combustion for approximately 3 seconds at altitudes between 35 and 29 kilometers. The experiment utilized a double wedge intake and two back-to-back constant area combustors, one fueled with hydrogen and the other unfueled, to compare the performance and validate theoretical models. The flight data showed a reasonable correlation with preflight shock tunnel tests, providing crucial validation for the use of short-duration ground test facilities for scramjet development.

1.2.3 X-43 Hyper-X

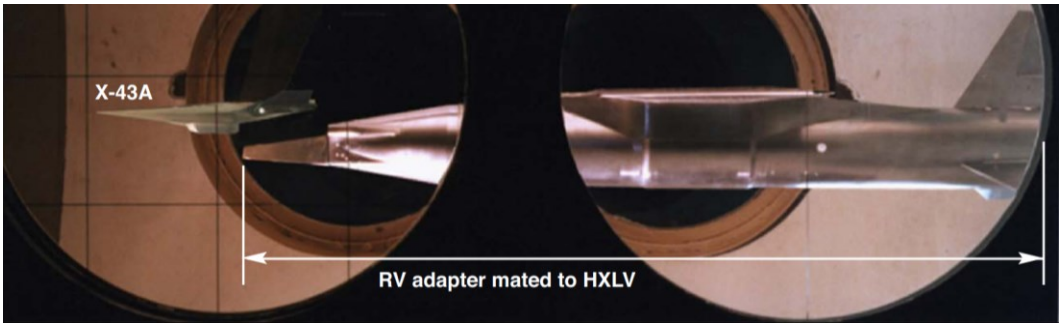

Figure 1.5: The AEDC stage separation wind tunnel test models [7].

The X-43A, a part of NASA's Hyper-X program, represented a significant leap in hypersonic flight technology. The X-43A was launched from a modified Pegasus booster rocket, which carried it to its test altitude and speed. Once the desired altitude and speed were reached, the X-43A separated from the booster and ignited its scramjet engine. Three flights in total provided critical data for refining computational models, airframe structures, and attitude control [7]. In its third and final flight on November 16, 2004, the X-43A achieved a speed of Mach 9.6, approximately 7,000 miles per hour, at an altitude of around 110,000 feet. It cruised at nearly 40% the velocity of the ISS for just 10 seconds.

1.2.4 X-51 Waverider

Figure 1.6: X-51A Waverider mounted under the B-52 Stratofortress [8].

The X-51A Waverider's design focused on advancing scramjet engine technology using hydrocarbon fuel. Constructed by Boeing's High Desert Assembly, Integration & Test division, and powered by a scramjet engine from Pratt & Whitney Rocketdyne, the X-51A featured a sophisticated airframe and engine composed of a variety of exotic metals and ceramics designed to sustain significant heat load during long burns [9].

The vehicle's complex structure included a booster, interstage, and a cruiser, designed for non-recoverable flight demonstrations. At an altitude of about 50,000 feet and Mach 0.8, a B-52 drops the X-51. A solid rocket booster accelerated the vehicle to approximately Mach 4.8, after which the scramjet engine would ignite to propel it to Mach 5.1. The scramjet engine, initially powered by ethylene before transitioning to JP-7, accelerated the vehicle to hypersonic speeds, maintaining air-breathing flight for a record 210 seconds. The X-51A Waverider achieved a significant milestone with the vehicle traveling more than 230 nautical miles in just over six minutes and reaching a peak speed of Mach 5.1 [10-11].

1.2.5 Hypersonic Air-breathing Weapon Concept (HAWC)

Figure 1.7: Artist's concept of Hypersonic Air-breathing Weapon Concept (HAWC) [12].

The Hypersonic Air-breathing Weapon Concept (HAWC) program is a collaborative initiative between the Defense Advanced Research Projects Agency (DARPA) and the United States Air Force (USAF). The program aims to develop and demonstrate the technologies necessary to create an effective and affordable air-launched hypersonic cruise missile. Operating at speeds of Mach 5 and beyond, hypersonic systems promise longer ranges, shorter response times, and enhanced effectiveness for future U.S. military operations, particularly as adversary capabilities continue to advance. The primary objectives of the HAWC program include developing advanced air vehicle configurations capable of efficient hypersonic flight, utilizing hydrocarbon scramjet-powered propulsion to sustain hypersonic cruise speeds, and creating methods to manage the extreme thermal stresses encountered during high-temperature hypersonic flight [13]. Additionally, the program emphasizes the importance of affordable system designs, ensuring the missile system is cost-effective to produce and maintain. HAWC focuses on three critical technology challenge areas, also known as program pillars: air vehicle feasibility, effectiveness, and affordability.

The HAWC program has made significant progress, marked by several successful flight tests. The first Raytheon Technologies HAWC flight occurred in September 2021, achieving its test objectives [12-16]. Subsequent tests included another successful free flight in early July, leveraging data from previous tests to further explore the flight and scramjet engine operating envelopes. During these flights, the missile, powered by a Northrop Grumman scramjet engine, reached speeds greater than Mach 5, traveled over 300 nautical miles, and attained altitudes exceeding 60,000 feet. These advancements offer several strategic benefits, such as evading defenses and conducting rapid strikes, which provide a significant tactical advantage. The program's flight test data will be shared with the Navy and Air Force to aid in the development of future high-speed weapons, ensuring the U.S. maintains a strategic edge in global defense.

1.3 Space Access and Energy

We need a way to *accelerate* a craft from 0 to nearly 8 km/s (~Mach 25) to bring it into orbit around Earth. Using an air-breathing propulsion method for the majority of acceleration and elevation to orbit could significantly increase the performance of a launch vehicle due to the advantage in specific impulse of scramjets over rockets (Figure 1.1 & 1.8). Comparing different types of propulsion systems can illustrate the point of hypersonics far exceeding the specific impulse of conventional chemical rockets, while maintaining similar thrust capability. While many fuels can be used by either rockets or scramjets, rockets also must carry their own oxidizer. As chemical rocket propulsion continues to reach maturity, more focus may be placed upon taking advantage of scramjet technology.

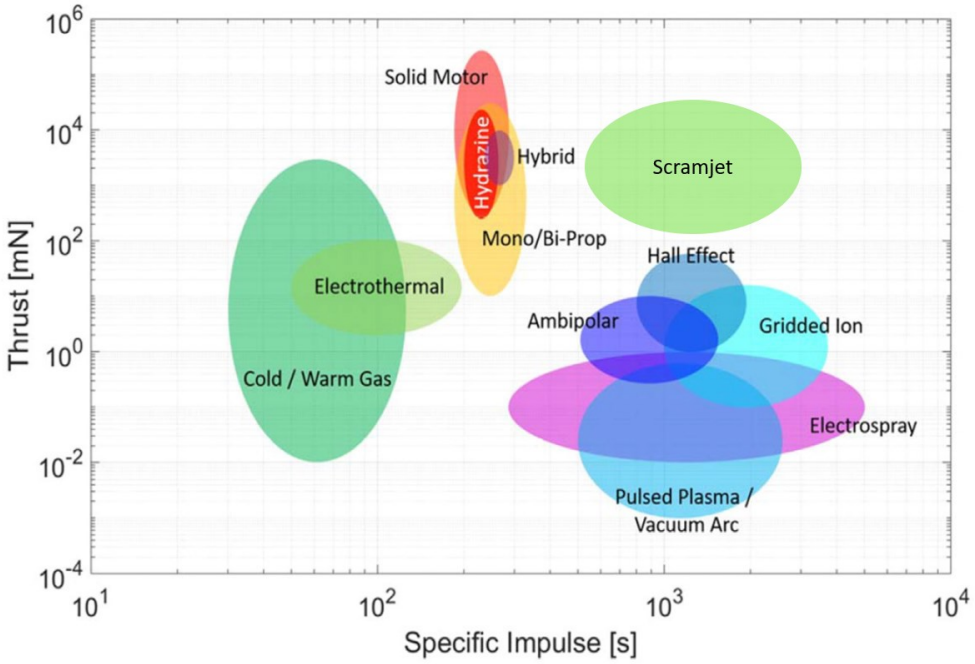

Figure 1.8: Spacecraft in-space propulsion trade space (thrust vs. specific impulse) [18].

1.4 Demand for Ground Testing Facilities

Wind tunnels serve as a crucial tool for several aerospace-related research areas. Their applications span across aerodynamics, atmospheric re-entry studies, development of advanced propulsion devices and material testing. They provide researchers with the capability to simulate and examine the effects of different flow conditions on objects or phenomena in a controlled and repeatable environment without costly rocket boosters.

The X-43A program cost nearly $230 million, yielding approximately 20 seconds of engine test time [19], which translates to around $11.5 million per second of engine data. In contrast, wind tunnels can produce repeatable flow conditions at a significantly lower cost. Integrating sensors on flight vehicles is far more challenging and expensive, whereas more detailed research can be conducted in wind tunnels. The X-51 experienced issues such as inlet instabilities; interactions between thermal radiation, shockwaves, boundary layers, and material stress which impacted downstream flow path and combustor conditions, ultimately causing some vehicles to fail [9]. These complex mechanisms are better suited for ground testing to understand the intricacies of their interactions.

Chapter 2 Supersonic Wind Tunnels

2.1 Supersonic Flow

To understand supersonic combustion, one must build up from the fundamentals of compressible flow theory. In low-speed incompressible fluids, it is assumed that the density of fluid does not change as it flows around any object. This is due to the relatively high speed of molecular collisions (~340 m/s at sea level) in the fluid relative to the speed of the fluid itself, or the ratio of internal energy to kinetic energy. Sonic speed, or Mach 1, is the speed of molecular collisions in a fluid (i.e., it represents the speed at which information is transmitted through the fluid via collisions). Beginning at a Mach number of near 0.3, fluid begins to show signs of compressibility, and the obvious effects of compressibility, like shockwave formation, are commonly present in aircraft as the Mach number passes 0.8 as seen in Figure 2.1 b) & c).

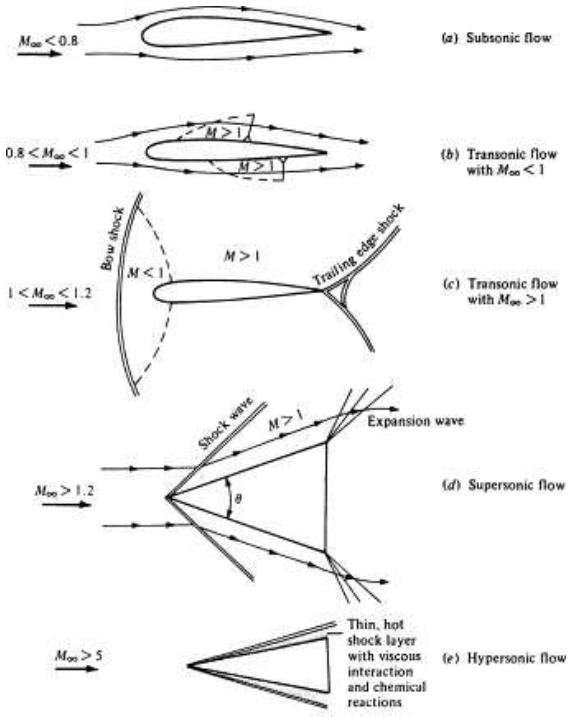

Figure 2.1: Regimes of flow from subsonic to hypersonic around aerodynamic bodies [20].

2.2 Role of Wind Tunnels

Whether it's studying the fluid dynamics of a new fighter jet or understanding the intricacies of heat transfer during the re-entry of spacecraft, wind tunnels offer invaluable insights. Depending on the application, various types of supersonic testing facilities are employed to simulate and understand different flow conditions. Wind tunnels are commonly thought of as being used to simulate the aerodynamic flow regimes over an object. However, they are also employed to study the internal flow of supersonic combustion ram jet (scramjet) engines. Typical examples of external flow experiments include aircraft stability, aeroelastic phenomenon, and re-rentry capsules. Internal flow experiments include isolators, combustors, and nozzles.

Previous research on laser ignition inside supersonic combustible mixture has shown promising results. McGann et al. have performed laser ignition studies inside of a the RC-19 direct-connect facility at the Air Force Research Laboratory [21]. Their experiments were performed in ethylene-air mixtures inside a cavity-flame holder-type combustor inside a Mach=3.0 free stream flow. They were able to determine the optimal ignition locations inside the cavity. By analyzing the light from the laser spark through a spectrograph and looking at the atomic oxygen and H-alpha emission lines, they were able to map the fuel-to-air ratio throughout the cavity. A similar study performed by Yang et al. have shown that plasma-induced flow recirculation can be used to anchor the flame inside the cavity flame holder [22]. Moreover, additional energy deposition via a secondary pulse was noted to accelerate the stabilization process. Brieschenk et al. proposed the idea of using a laser discharge to operate a scramjet in a radical farming configuration in which the plasma breakdown takes place in the inlet [23-24]. As the ionized fuel-air mixture moves through the isolator the hot pockets/radical farms created by the laser discharge further grow until the reach the main combustion chamber and ignite the main combustion zone. Such a configuration

would not necessarily require a cavity flame holder.

In the supersonic wind tunnel developed at Colorado State University we plan to test our resonant dual-pulse pre-ionization laser ignition technique. As shown in our previous studies, the technique enables great control over the early flame kernel dynamics [25-26]. The technique consists of a UV pulse that is resonantly tuned to pre-ionize molecular oxygen inside the air stream. A subsequent near-infrared pulse is spatially overlapped to add energy into the pre-ionized gas in a controlled fashion. Our facility will serve as a versatile research platform for these fundamental studies of ignition and flame stabilization inside a scramjet engine.

2.3 Types of Supersonic Wind Tunnels

Each type of supersonic wind tunnel, including the closed loop, shock tube, Ludweig tube, blowdown, and indraft, offers a unique set of advantages and disadvantages, depending on the specific research or testing needs.

2.3.1 Closed-loop facility

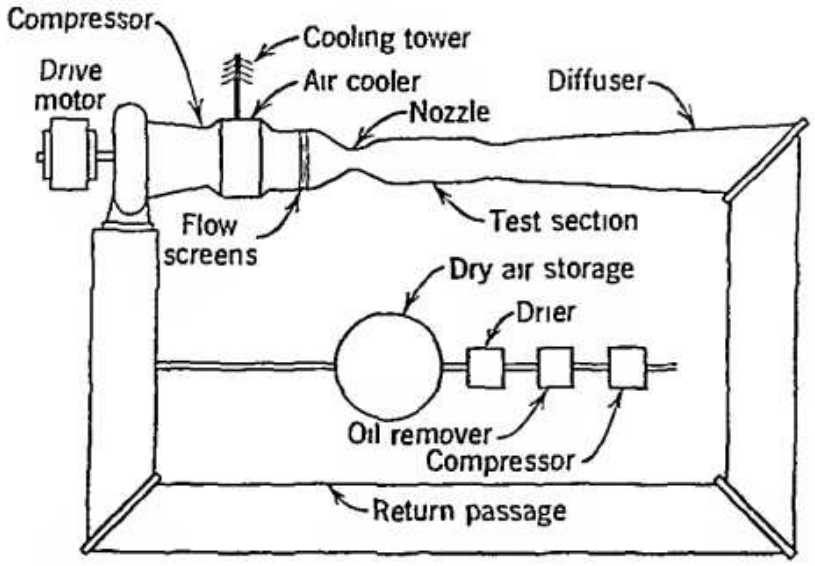

Figure 2.2: Diagrammatic layout of closed-circuit, continuous flow, wind tunnel [27].

While closed loop tunnels are more common and practical for subsonic and transonic testing, hypersonic testing facilities, such as those run by NASA [28-30], are rare, large, complex, and prohibitively expensive. The requirement of maintaining a continuous supersonic flow increases construction cost, maintenance costs, more air conditioning equipment (Figure 2.2), and extremely high power. This limits practical use to around Mach 3.

For hypersonic testing, the more common approach is to use impulsive type facilities such as Ludwieg tubes and shock tubes. These facilities can generate the necessary flow conditions for hypersonic testing in a more cost-effective and manageable way, providing valuable data without the extensive infrastructure required by closed-loop wind tunnels.

2.3.2 Shock Tube

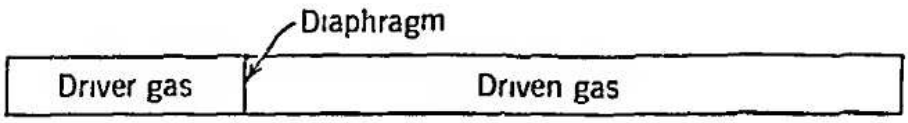

Figure 2.3: Shock tube diagram [27].

Shock tubes are experimental devices used to generate and study high-speed shock waves and their interactions with different materials and flow conditions. Essentially, a shock tube consists of a long, straight tube divided into two sections by a diaphragm. The high-pressure section, known as the driver section, contains a pressurized gas, while the low-pressure section, called the driven section, contains the test gas (Figure 2.3). When the diaphragm is ruptured, the high-pressure gas rapidly expands into the low-pressure section, creating a shock wave that travels down the tube. This controlled environment allows researchers to simulate and analyze the behavior of shock waves under various conditions based on the pressure, temperature, and composition of each gas.

Shock tubes have a wide range of applications, particularly in the field of aerodynamics and propulsion. They are instrumental in studying high-speed flows, such as those encountered in

hypersonic flight. By observing how shock waves interact with different surfaces and materials, researchers can gather valuable data on heat transfer, pressure distribution, and aerodynamic forces. This information is crucial for designing more efficient and robust airframes, engines, and other aerospace components that must withstand extreme conditions.

Beyond aerospace, shock tubes are also used in other scientific and engineering disciplines. For instance, they play a significant role in combustion research, where they help scientists understand the ignition and combustion characteristics of various fuels [31]. This knowledge is essential for developing advanced propulsion systems and improving fuel efficiency. Additionally, shock tubes are employed in materials science to investigate the behavior of materials under sudden and extreme loading conditions, providing insights into their strength, durability, and failure mechanisms.

2.3.3 Ludwieg Tube

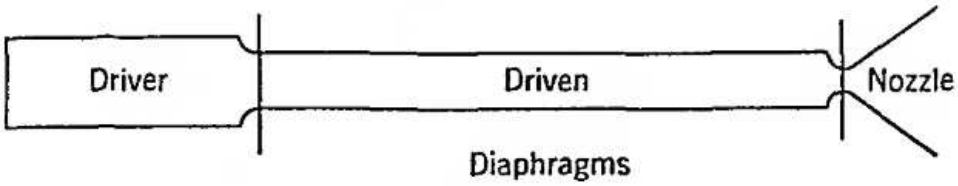

Figure 2.4: Schematic of shock tunnel [27].

A Ludweig tube is a specialized type of shock tube designed for generating high-velocity flows, often used in aerodynamics and propulsion research. This type of tunnel is characterized by a relatively steady flow, advantageous for aerodynamics experiments.

Unlike a conventional shock tube, a Ludweig tube incorporates an additional diaphragm and nozzle (Figure 2.4) to use the shock tube as a high-enthalpy source for a supersonic wind tunnel. [32] The tube is divided into three sections: the driver section, the driven section, and a nozzle via a secondary diaphragm. When the first diaphragm is ruptured, the high-pressure gas in the driver

section rapidly expands into the driven section like a conventional shock tube. The shockwave reflects off the secondary diaphragm creating a high temperature and pressure region of nearly stationary air adjacent to the nozzle, which ruptures the second diaphragm and starts the nozzle. The presence of the expansion section allows for the generation of a steady supersonic flow for a longer duration than typically achievable with a standard shock tube.

The primary utility of a Ludweig tube lies in its ability to produce high-speed, quasi-steady flows, which are valuable for studying aerodynamic properties and flow behaviors at supersonic and hypersonic speeds. This extended flow duration is particularly beneficial for testing and developing hypersonic vehicles, such as missiles, space re-entry vehicles, and high-speed aircraft, where understanding the aerodynamic forces and thermal loads over a sustained period is crucial.

However, the Ludweig tube also has its disadvantages. One significant limitation is its complexity and the associated costs. The setup requires precise control of pressures, diaphragm rupture, and the maintenance of a low pressure at the nozzle exit, which demands sophisticated equipment and meticulous operation. Additionally, the duration of the steady flow, while longer than that in conventional shock tubes, is still relatively short, typically in the range of milliseconds. [33-36] This limits the types of experiments that can be conducted and the extent to which results can be generalized to longer-duration flight conditions. Despite these challenges, the Ludweig tube remains a valuable tool for high-speed aerodynamics research, providing critical insights that contribute to the advancement of hypersonic technology.

2.3.4 Blowdown

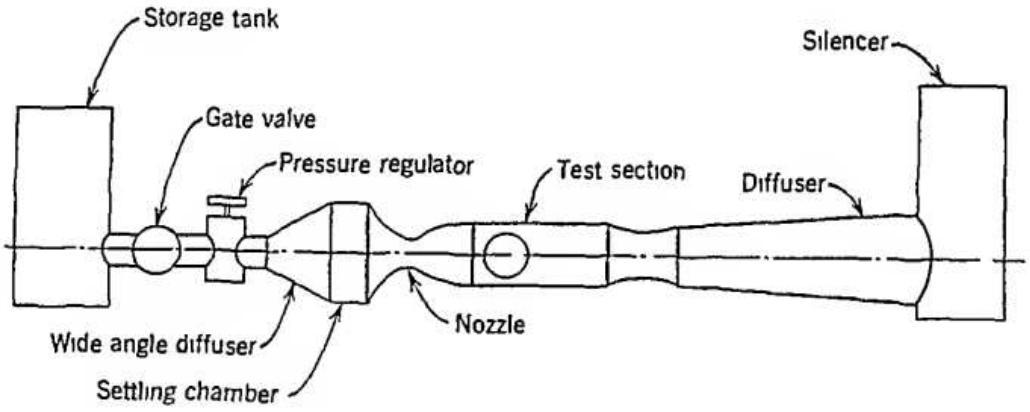

Figure 2.5: Diagrammatic layout of intermittent blowdown tunnel [27].

A blowdown tunnel can expand the operational envelope towards higher Mach numbers. The blowdown tunnel is the most widely used type of facility for scramjet engine research. It consists of two reservoirs at each end of the nozzle to create the required pressure differential to drive the flow (Figure 2.5). The inlet reservoir is typically at high pressures ($p_0 > 1$ atm) and the outlet reservoir acts as a dump tank for the flow coming out of the diffuser. When coupled with a high enthalpy source before the nozzle inlet (such as an arc jet or a vitiated air combustor) it can generate conditions amenable for combustion testing inside the test section. [37] However, the design can become expensive, including the necessity for large volumes of compressed air and vacuum, as well as a heating element. This requirement can be both costly and logistically challenging. Furthermore, the air supply necessitates recharge time between tests, thereby limiting the frequency of testing.

2.3.5 Indraft

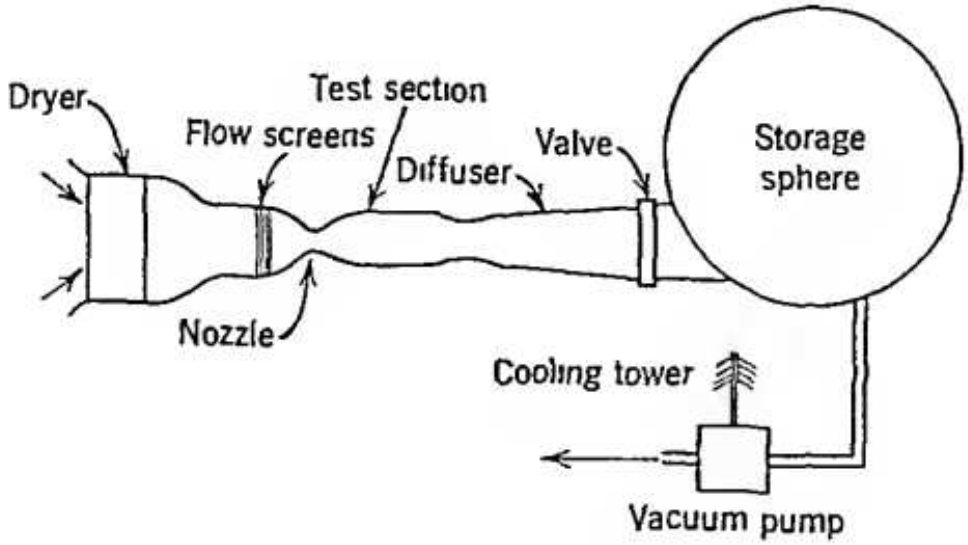

Figure 2.6: Diagrammatic layout of intermittent indraft wind tunnel [27]

The indraft tunnel is a sub-type of a blowdown tunnel, using atmospheric air as its intake. The addition of a vacuum chamber downstream of the test section is used to create a low-pressure region that draws air through the test section (Figure 2.6). This design is cost-effective and energy-efficient, allowing for the most constant flow conditions during the supersonic phase of the operation and enabling the study of combustion phenomena like a blowdown tunnel. The available experimental time is dictated by nozzle geometry (which controls the flowrate through the tunnel) and the size of the vacuum tank. This design type is less expensive than the classical blowdown tunnel and while it can only offer a narrow range of Reynolds number conditions, it is suitable for combustion testing in a direct-connect configuration with moderate heating. A similar configuration has been recently built at California Polytechnic State University to be used by their undergraduate students as a course supporting low-cost supersonic lab facility [38].

2.4 High Enthalpy Sources for Hypersonics

For scramjet propulsion, we need heaters to replicate flight conditions. Flying at high Mach numbers leads to very high stagnation temperatures in our atmosphere. Supersonic nozzles trade thermal energy for kinetic energy, and so as wind tunnels reach higher Mach numbers, the temperature requirement increases drastically. Various solutions for heating the air before a wind tunnel nozzle have different consequences for research in terms of gas composition and temperature equilibrium.

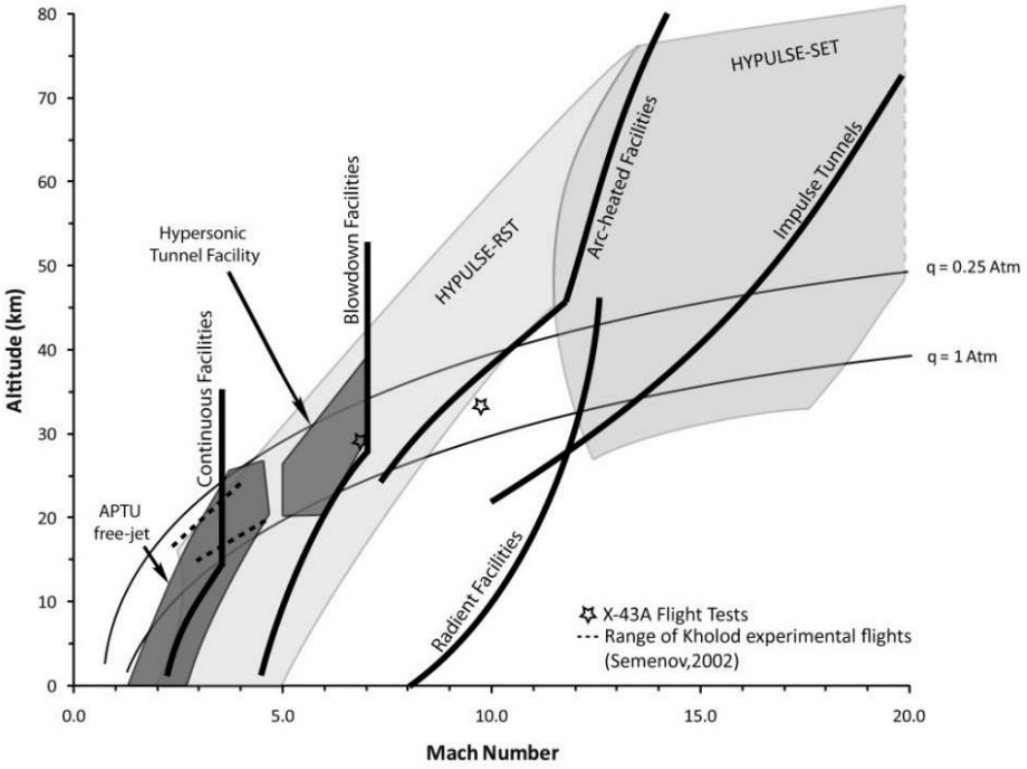

Figure 2.7: Air-breathing flight corridor and domain covered by existing facilities [39]

2.4.1 Piston Driven

Impulsive facilities utilize a piston to compress the working fluid to high temperatures and pressures. For high Reynolds number testing and even higher Mach number, shock tube driven facilities have been employed. As an example the T4 shock driven tunnel from University of

Queensland can reach testing Mach number as high as Mach=10 and total pressures P0=90 MPa [43], allow for testing at Reynolds numbers approaching a million.

While these facilities produce chemically non-reactive flow, they require a large physical footprint. The overall length of the high enthalpy shock tunnel Göttingen (HEG) in Germany is 62 meters, and it weights approximately 280 tons, a third of which is accounted for by an inert mass used to reduce the tunnel recoil [44]. The test duration ranges from 3 to 8 milliseconds at a temperature of 9900 K and produces a maximum Mach of 10.3. Such a facility is ideal for studying high enthalpy flows (such as atmospheric re-entry) but the test duration is too short to conduct detailed scramjet combustion testing.

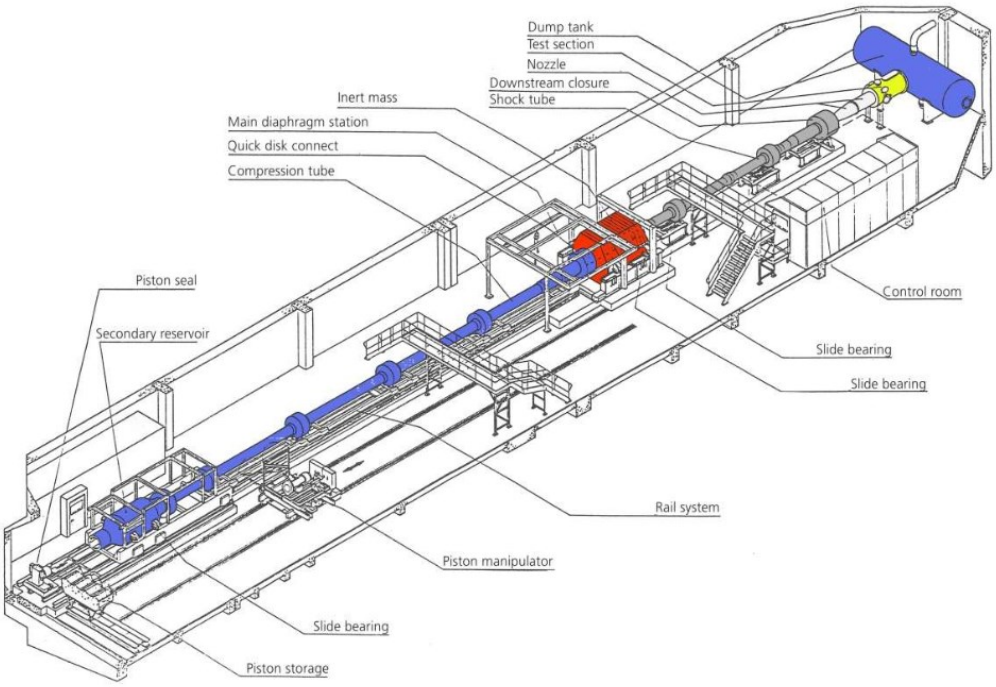

Figure 2.7: Diagram of HEG facility [44]

2.4.2 Electrically Heated

Electrically heated facilities use ohmic resistance and natural convection to raise the fluid temperature. While this is a simple design and produces clean flow, resistance heaters are large,

expensive, inefficient, and require high electric power. The dual-mode supersonic combustion facility at the University of Virginia uses a large-scale heater, which can operate for several hours and reach flow speeds of Mach 2 [45].

The SRB-50 wind tunnel at the University of Notre Dame utilizes industrial heaters in a plenum chamber and a high pressure charge tank upstream of the plenum chamber. The high pressure working fluid in the charge tank serves to compress the air being evacuated from the plenum section. Internal flow straighteners enhance the hot-cold boundary and create a high-pressure, cold-air piston to overcome adiabatic cooling due to rapid evacuation [46]. It is illustrated both computationally and experimentally that the charge tank provides larger exit temperatures due to decreased mixing of the replacement air to the plenum section as it is being evacuated. This facility serves as inspiration during the CSU wind tunnel design.

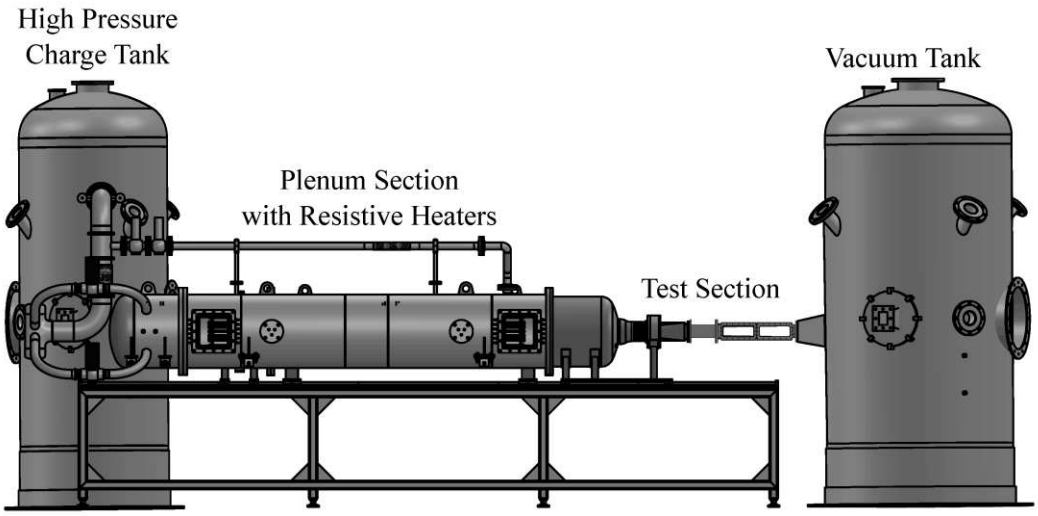

Figure 2.8: Overview of the SBR-50 facility with major components labeled [46]

2.4.3 Vitiated Air

Combustion heated facilities achieve high enthalpy flow by burning natural gas or hydrogen in the air stream. This can provide a large, continuous, heated flow while minimizing cost and complexity. However, the maximum temperature is limited by the fuel's adiabatic flame

temperature and the working fluid is comprised of combustor exhaust gases (as opposed to air). Thid type of facility has a moderate implementation cost but the vitiated nature of the flow means that complex calibration and modeling needs to be performed to correlate wind tunnel results with flight behavior [41-42]. The direct-connect supersonic combustion research facility at the U.S. Air Force Research Laboratory in Ohio can achieve continuous airflow of 13.6 kg/s at p0=5.17 MPa, and a maximum temperature of 922 K, with 20.7 kPa continuous exhaust. The facility provides flow condition corresponding to flight Mach numbers between 3.5-7.0. [47-48]

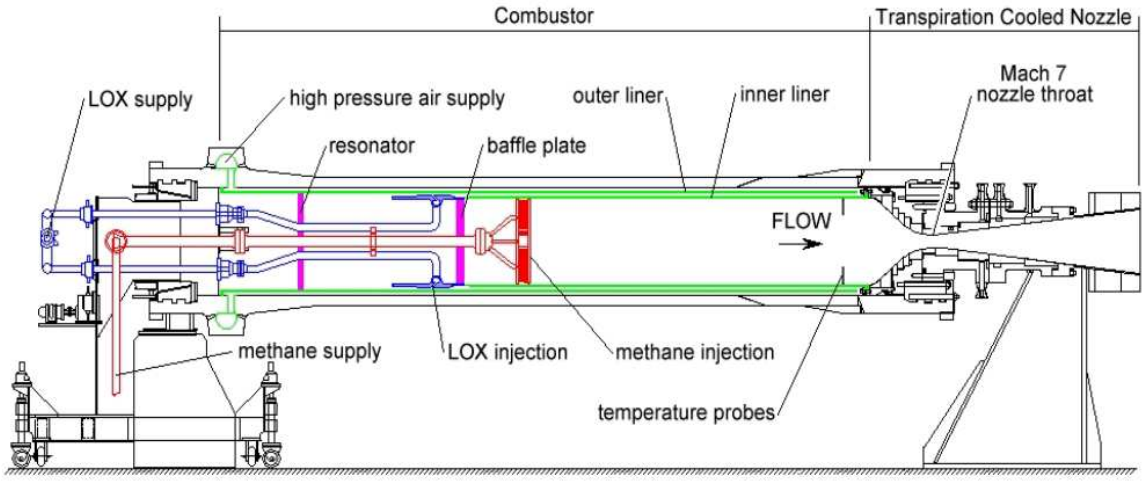

Figure 2.9: NASA Langley 8-Foot High Temperature Tunnel Mach 7 Burner [47]

2.4.4 Arcjet

Arc-heated facilities generate plasma discharge to raise the inlet temperature. A typical facility will utilize a power supply to apply a high voltage between an anode and a cathode, which will initiate an arc via air breakdown. As an example, NASA's Langley Research Center operates a hypersonic arc-heated tunnel to duplicate true flight stagnation enthalpy conditions, typical for a flight Mach number range of 4.7 up to 8. To generate the necessary high enthalpy flow, a portion of the incoming air is heated by a 13 MW electric arc to a bulk temperature of approximately 4000 K. Its main advantage is that it can be run quasi-continuously. The facility has been in service since 1976 and

was used for various air-breathing propulsion testing platforms [40-42].

The maximum temperature in arcjets is significantly higher than many other high enthalpy source; however, these facilities are expensive to construct due to their complexity and expensive to maintain due to their fast-eroding electrodes. [27] The pulsed-arc-heated hypersonic wind facility at the University of Notre Dame can provide stagnation temperatures of 2000-3500 K to produce hypersonic flows at Mach 9 for a maximum test duration of 1 second [49]. The absolute pressure at the electrodes must be below 0.7 MPa to initiate the arc.

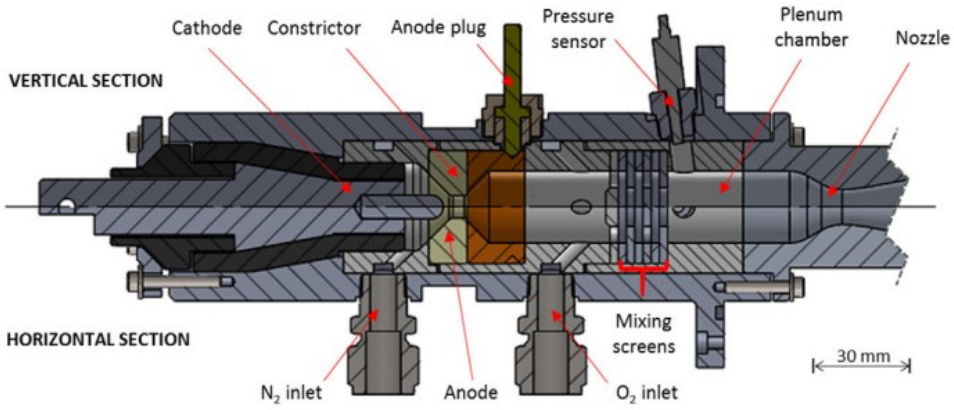

Figure 2.10: ACT-I Facility diagram [49]

Table 2.1: Supersonic wind tunnel list (Credit: Plese 2024)

Facility	Location	Type of Heating	Power	Mach	T_0 (K)	p_0 (MPa)	Test Time
	Colorado State U.			**2.5-7**	**300**	**0.085**	**0.5-7s**
HEAT	Alta	Electric Arc					
ACT-I	U. of Notre Dame	Electric Arc	260 kW	4.5–9	2000–3500	< 0.3	~ 1 s
ACT-II	U. of Notre Dame	Electric Arc	250 kW				400–600 ms
AHSTF	NASA Langley	Electric Arc	13 MW	4.7–8	1100–2900	< 4.6	Cont.
F4	ONERA	Electric Arc	150 MW			50	~ 400 ms
4T	ADEC	Electric Arc		0.2–2			Cont.
SCIROCCO	CIRA	Electric Arc	70 MW	6–12	2000–10000	0.1–1.7	30 min
SBR-50	U. of Notre Dame	Electric Resistance	67 kW	2,4,6	300–755	0.1–0.4	0.5–2 s
HTF	NASA Glenn RC	Electric Resistance	3 MW	5–7	1220–2755	0.48–8.27	5–300 s
HWT	Sandia EAF	Electric Resistance	3 MW			< 21	
TWT	Sandia EAF	Electric Resistance		0.5			~ 30 s
RC-19	WP-AFB	Electric Resistance		1.5–5	< 922		Cont.
UVaSCF	U. of Virginia	Electric Resistance	300 kW	2,3	1200	0.3	Cont.
UF	U. of Florida	Electric Resistance Combustion (H_2/O_2/Air)	1.2 MW	5.5–6.5	1300–1800		Cont.
DCSCTF	NASA Langley	Combustion (H_2/O_2/Air)		7.5	< 2100	< 0.68	20–50 s
CHSTF	NASA Langley	Combustion (H_2/O_2/Air)		3.5–6	< 1700		
8 Ft. HTT	NASA Langley	Combustion (CH_4/O_2/Air)		4–7	700–2200	0.35–13.8	25 s
RC-18	WP-AFB	Combustion		2.2	< 922	< 4.8	Cont.
RJTF	JAXA Kakuda	Combustion		4–8	< 2600	0.7–10	Cont.
HEG	DLR Gottingen	Free-Piston Driven		5.7–10.3	1640–9900	200	3–8 ms
T3	Australian National U.	Free-Piston Driven					
T4	U. of Queensland	Free-Piston Driven		4–10	3000–3500	< 80	0.5–5 ms
ET	Stanford U.	Expansion Tunnel		2.4–4.7	3000–3500	10–15	< 0.5 ms
X3	U. of Queensland						
HYPULSE	NASA Langley	Expansion Tunnel		7-19	6000-11000	<27	
TWT	CALSPAN			0.1–1.3			

Chapter 3 CSU Supersonic Wind Tunnel Design

3.1 Design Overview

Our custom-built wind tunnel is developed with the objective of investigating the physics of scramjet engines. The facility allows us to study various inlets, shockwave interactions inside isolators, and combustion at supersonic conditions.

This chapter has been split into two main sections, gasdynamic design and mechanical design. The gasdynamic design section discusses the quasi-1D code developed to better understand the required flowrates and test section sizes to achieve desired experimental testing times, the method of characteristics used to shape the shock-free de Laval nozzle, and the CFD simulations performed to characterize the flow throughout the entire tunnel. The mechanical design section describes how the inlet, test section, and vacuum system were designed. This includes general CAD schematics and stress analysis.

One of the key results of this project is the behavior of shockwaves around a wedge in supersonic Mach 2.5 flow. Synthetic schlieren from computations results clearly show the structure of these shockwaves, which are critical for understanding the behavior of scramjet engines. The fact that the transient computational model of the wind tunnel test section was able to capture this phenomenon is a good indication that the tunnel's flowpath is designed properly and should proceed with physical testing.

The highly modular nature of the CSU wind tunnel design is significant for its utility in years to come. It allows for easy reconfiguration and testing of different geometries, making it a versatile tool for investigating a wide range of supersonic flows. While the cooling system was not designed for continuous duty, it is able to effectively cool the pump while bringing the chamber pressure

down between experiment runs. The iterative design process used for the wind tunnel test section and its associated diagnostics was a key factor in the success of the project. This process allowed for continuous improvement and refinement of the setup, ultimately resulting in a highly accurate and reliable tool for investigating supersonic flows.

The tunnel is designed to be operated in three main configurations. We will initially use it to study the supersonic flow around wedges (Figure 3.1 top) and other aerodynamic probes. These types of tests will be used to characterize the flow inside the tunnel and confirm the desired Mach number in the test section. The second is a direct-connect configuration (Figure 3.1 bottom), where the modular mounting system of the test section is used to mount cavity flame holders, fuel injectors, ignitors, etc. to emulate the inner flow channel of a scramjet engine.

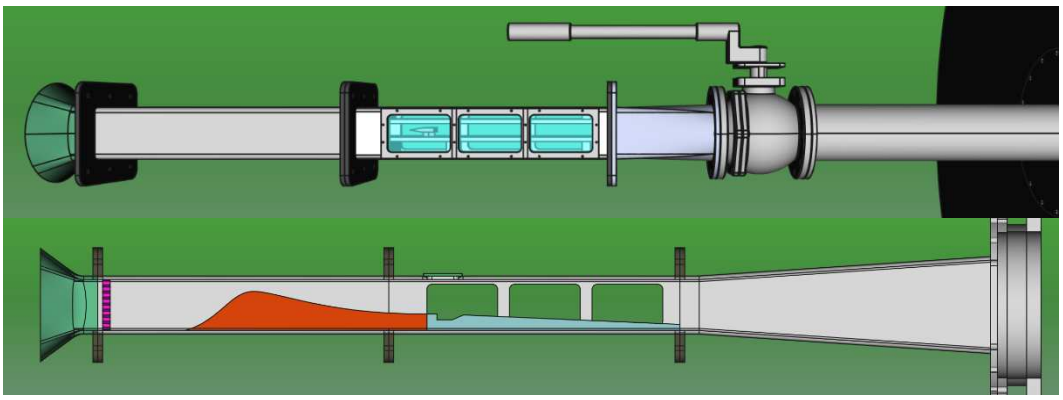

Figure 3.1: 3-D rendering of the CSU indraft wind configurations: external-flow with wedge installed (top) and the direct-connect configuration featuring a cavity flameholder (bottom)

In the future we will also use the tunnel in a combined external/internal flow configuration where a model of a full scramjet intake, isolator, combustor, and aft body are placed in the wind tunnel to obtain more detailed information on the operation of a scramjet.

3.2 Gasdynamic Design

3.2.1 Quasi 1-D Model of the Wind Tunnel

A quasi-1-D code based on the isentropic relations inside a converging-diverging nozzle was used to obtain a preliminary correlation between the test size, mass flowrate and experimental time. The program uses the following entry parameters: the atmospheric pressure, p_0, atmospheric temperature, T_0, vacuum chamber volume, V, specific heat ratio of air, γ. The code runs over various scenarios based on the pressure ratio between the inlet (atmosphere, in our case) and the vacuum tank. As the tank gradually fills, the flow through the converging-diverging nozzle goes through different regimes: under-expanded, over-expanded, design condition, shock-in-nozzle (non-isentropic), and finally subsonic. In our case, the wind tunnel testing can be performed if the pressure ratio is low enough to prevent the formation of shocks inside the diverging side of the nozzle.

The time required to fill the dump tank can be calculated directly from the continuity equation and, after some manipulation, it yields:

$$t = \frac{P_{end}V}{\dot{m}RT_0} \tag{3.1}$$

Where V=3.5 m^3 represents the tank volume, T_0=300 K is the stagnation temperature, R is the gas constant and $\dot{m}$ is the mass flowrate through a choked nozzle given by:

$$\dot{m} = \frac{p_0 A_{thr}}{\sqrt{R_g T_0}} \sqrt{\gamma} \left(\frac{2}{\gamma+1}\right)^{\frac{\gamma+1}{2(\gamma-1)}} \tag{3.2}$$

Finally, $P_{end,}$ represents the dump tank pressure at which the tunnel begins to unstart due to the presence of a shock wave inside the nozzle. This exit shock condition is determined via:

$$P_{end} = \frac{p_{02}}{p_{01}} \frac{p_e}{P_{0e}} p_{01} \tag{3.3}$$

Where the total pressure loss across the shock, p_{02}/p_{01} is computed using the normal shock relations as a function of the upstream supersonic Mach number, Ma_1:

$$\frac{p_{02}}{p_{01}} = \left(\frac{(\gamma+1)Ma_1^2}{(\gamma-1)Ma_1^2+2}\right)^{\frac{\gamma}{\gamma-1}} \left(\frac{\gamma+1}{2\gamma Ma_1^2-(\gamma-1)}\right)^{\frac{1}{\gamma-1}} \tag{3.4}$$

And the ratio of the exit pressures is computed using the isentropic relations:

$$\frac{p_e}{p_{oe}} = \left(1 + \frac{(\gamma-1)Ma_1^2}{2}\right)^{-\frac{\gamma}{\gamma-1}} \tag{3.5}$$

In this case for an ideal nozzle at Mach=2.5 with a test section size of 1.57 x 5.25, the quasi 1-D code predicts a flowrate 0.41 kg/s, where a shock establishes at the nozzle exit for a dump tank pressure of P_{end}=0.36 atm (note: in Fort Collins, CO, P_0=0.85 atm). This yields an experimental time of t ~ 2.5 seconds. Figure 3.2 below presents a parametric study that shows how the wind tunnel test time changes as a function of the desired test section Mach number for various test section heights (as discussed in the next section, we always keep the width of the test section to 5.25" but we can change its height using two mounting plates and spacers). The results show that, for a given test section height, the test duration slightly increases as a function of the Mach

number. This is because, to increase the Mach number, one reduces the sonic throat area, A*, which reduces the flowrate.

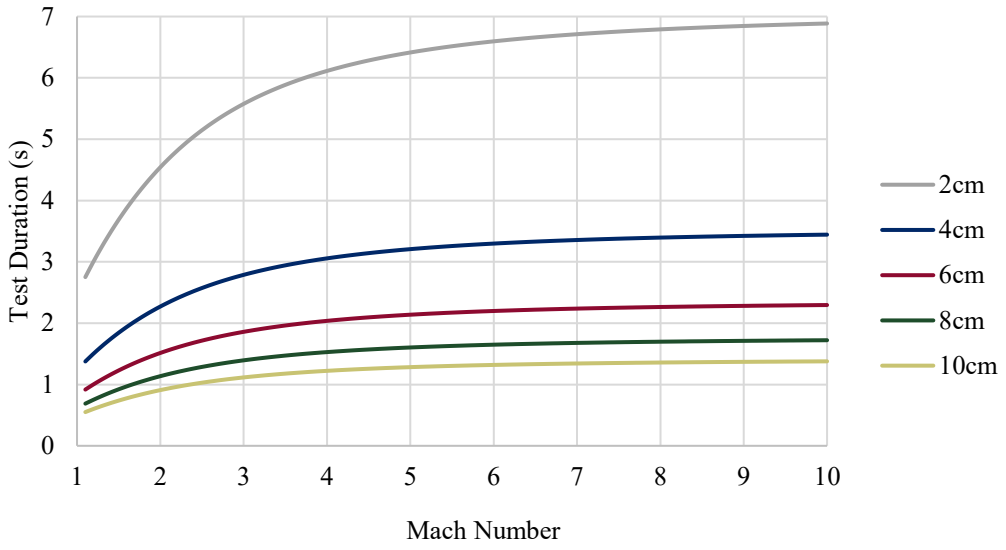

Figure 3.2: Maximum test durations for various Mach numbers and nozzle sizes

This leads to a decrease in flowrate at choked conditions as shown in Eq. (3.2). Another important aspect analyzed with the quasi 1-D model was the variation of the test section temperature as a function of the desired wind tunnel design Mach number. Given our focus on future combustion testing it is important to ensure that test section conditions will allow for combustion reactions to take place. Test temperature is calculated using the isentropic relationship between stagnation temperature and temperature at the exit of the nozzle:

$$T_e = T_0 \left(1 + \frac{(\gamma-1)Ma_e^2}{2}\right)^{-1} \tag{3.6}$$

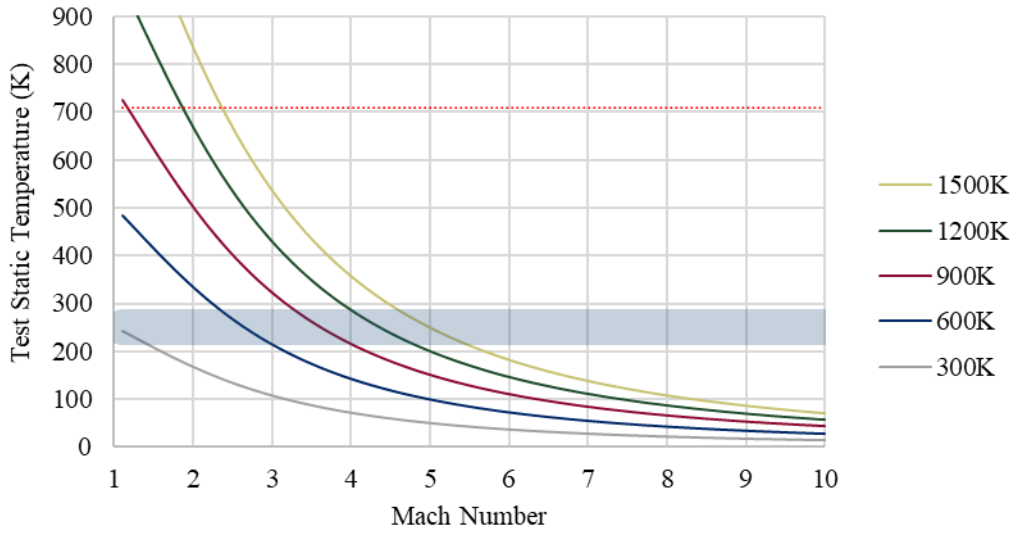

Figure 3.3: Wind tunnel flow temperature at various Mach numbers and total temperatures

As shown in Figure 3.3 above, an increase in wind tunnel Mach number leads to considerable cooling of the air. This is because as the fluid is accelerated through the converging-diverging nozzle, the thermal energy of the relatively stagnant air is being converted into kinetic energy. The noted significant gas cooling can lead to water condensation and gas liquefaction and it restricts the wind tunnel operation to relatively low Mach numbers even without combustion testing. For ignition studies, a desirable test section temperature should be at least 300 K. To achieve this at a flow Mach number of 2.5 one needs to heat up the tunnel to around 700 K. To achieve the required upstream temperature conditions, the wind tunnel must be retrofitted with a heating module. Existing wind tunnels use various solutions such as: shock tubes, vitiated air, electric resistors, and arcjets, as discussed in section 2.4. We used the quasi 1-D analysis to size the required heater for our wind tunnel. Heating power is simply calculated based on the knowing the required gas temperature increase to be generated by the heater, T, and the choked flowrate of the tunnel,

$$Q = \dot{m}\bar{c}_p\Delta T \tag{3.7}$$

The specific heat is evaluated at the average temperature between the inlet and the test section. The required heating power for maintaining a test section temperature of 300 K as function of Mach number and test section height is shown in Figure 3.4 below. The non-linear behavior observed is explained by two competing mechanisms. As the Mach number increases the flow rate decreases for a fixed test section height. At the same time, the additional flow acceleration (and subsequent gas cooling) leads to an increase in the required stagnation temperature. Nonetheless, above transonic Mach numbers (Ma > 1.7) the trend is dictated by the flow rate. If one were to try to maintain the same flowrate at various Mach numbers, of course, things would look more intuitive.

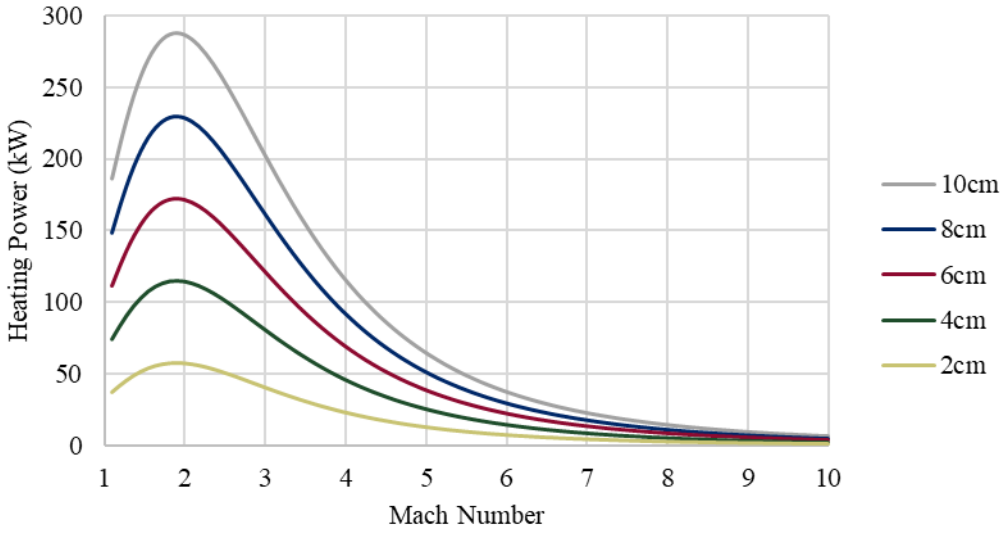

Figure 3.4: Required heating power for a 300 K static temperature flow at various Mach numbers and nozzle sizes for the CSU wind tunnel

Figure 3.5 shows altitude, airspeed, and dynamic pressure of various aircraft, along with the current and future capabilities of CSU wind tunnels. The current CSU wind tunnel configuration (depicted by the brown line) can replicate conditions up to a certain range of altitudes and speeds,

but it may not cover the entire flight envelope of advanced hypersonic vehicles like the X-51 and X-43, which operate at higher speeds and altitudes. The planned CSU wind tunnel (shown by the purple line) extends this range with a high-side pressure of (1.1 MPa at 3000 K) instead of today's indraft (84 kPa and 300 K), indicating an improved capability to match the flight enthalpy and dynamic pressures required for scramjet research. This development is crucial for advancing our understanding and performance of hypersonic propulsion systems, ensuring that experimental data is valid and applicable to real-world scenarios.

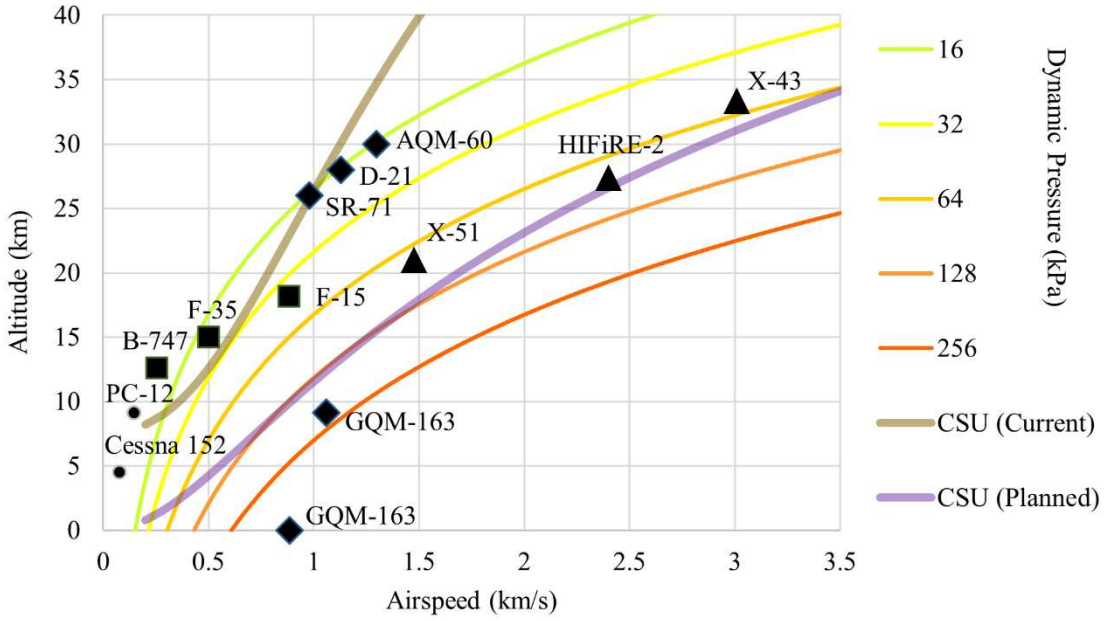

Figure 3.5: Comparison of various aircraft's altitude, airspeed, and dynamic pressure with the current and future CSU wind tunnel capability

Flight enthalpy is a crucial parameter in hypersonic propulsion research, particularly for scramjets, as it represents the total energy content of the incoming airflow. This energy comprises both the kinetic energy due to the high velocity of the aircraft and the thermal energy of the air itself. Achieving the correct flight enthalpy in a ground-based wind tunnel is essential to simulate real flight conditions accurately. If the enthalpy is not correctly matched, the combustion process

in the scramjet may not occur as it would in actual flight, leading to inaccurate data and potentially flawed research outcomes.

Dynamic pressure, which is the kinetic energy per unit volume of a fluid particle, also plays a significant role in wind tunnel testing. It influences the density and pressure of the airflow entering the scramjet engine. Different dynamic pressures can alter the behavior of the airflow, affecting the mixing and ignition processes within the scramjet. Therefore, wind tunnels must be capable of not only matching the flight enthalpy but also reproducing the appropriate dynamic pressures experienced at various altitudes and speeds. This ensures that the conditions under which the scramjet operates in the tunnel are as close to real-world conditions as possible.

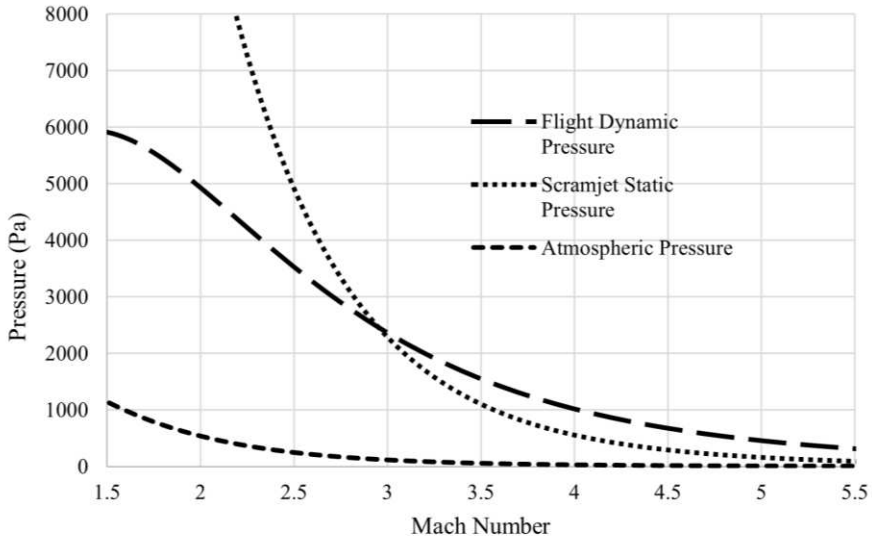

Figure 3.6: CSU indraft tunnel combustor, dynamic, and stagnation pressures for a 20:1 compression scramjet in a direct-connect experimental setup varying in combustor Mach number

Figure 3.6 shows the relationship between pressure and Mach number for three key types of pressure relevant to scramjet engines: flight dynamic pressure, scramjet static pressure, and atmospheric pressure. As Mach number increases, flight dynamic pressure and scramjet static pressure both decrease significantly, while atmospheric pressure decreases more gradually.

As the CSU supersonic wind tunnel is upgraded, it will allow for precise adjustments of Mach number and pressure, enabling detailed study and optimization of scramjet performance under various conditions without the variability, risk, and low weights associated with flight tests.

3.2.2 CFD Modeling Overview

The motivation for performing detailed computational fluid dynamics was to better understand the inner flow of the tunnel. In particular, we wanted to verify that the nozzle designed by the method of characteristics in the previous section is indeed operating shock-free at the design Mach number. Steady state and transient simulations of the entire wind tunnel flow channel were performed using ANSYS Fluent. A schematic of the problem setup is shown in Figure 5 below. The flow was solved using a density-based solver on a 2-D mesh consisting of 800,000 cells with increased fidelity around areas of interest. For the tunnel inlet we used a pressure-far field boundary condition which corresponds to ambient conditions in Fort Collins, CO p0=0.84 atm. For the outlet the vacuum the dump tank pressure was fixed to 0.05 atm (corresponding to the design condition inside the nozzle).

Figure 3.7: Supersonic wind tunnel 2-D unstructured mesh and Mach number contour

The resulting Mach contour, shown in Figure 3.8 above, confirms the accuracy of our nozzle design via the method of characteristics. The flow accelerates up to a Mach ~ 2.5 at the nozzle exit

as expected. In addition, a developing boundary layer is observed along the tunnel walls. For the small tunnel height configurations (1.7”) there is no need for a diffuser because the flow decelerates sufficiently once the boundary layers connect downstream of the test section. To confirm that the flow is unperturbed throughout the nozzle, the density contours obtained from the ANSYS Fluent simulation were further post-processed to generate a synthetic schlieren image of the nozzle flow (Figure 3.9).

3.2.3 Supersonic Nozzle Gasdynamic Design

3.2.3.1 Nozzle Geometry – Method of Characteristics

The method of characteristics is a mathematical technique used to design the contour of the diverging section of the nozzle to ensure smooth and efficient supersonic expansion. This method helps in managing the complex interactions within the supersonic flow, such as shock waves and expansion waves, by determining the optimal shape for the nozzle. In supersonic flow, small disturbances propagate along characteristic lines, which are paths determined by the Mach angle. The method of characteristics uses these lines to map the flow field, ensuring that changes in velocity and pressure occur smoothly. As the flow expands through the diverging section, it encounters an expansion fan, a series of infinitesimal expansion waves that cause the flow to accelerate. The method of characteristics helps design the nozzle shape to align these expansion waves correctly, preventing the formation of shock waves that would reduce efficiency. The supersonic contour of the nozzle is shaped based on the characteristic lines, ensuring that the flow expands smoothly and uniformly. When applying the MOC to the design of a supersonic wind tunnel nozzle the main objective is to find the optimal nozzle contour such that the flow entering the test section is uniform and parallel. MOC can only be used for the diverging/supersonic part of the nozzle. This precise shaping minimizes total pressure losses and maximizes the kinetic energy of the exhaust flow,

resulting in higher thrust efficiency.

The basis of this method represents an approximation to the Navier- Stokes conservation equations assuming an isentropic, inviscid and irrotational flow. Applying the MOC leads to the reduction of the partial differential equations that describe the flow through the nozzle to a set of compatibility equations that allows us to determine how the flow evolves over characteristic directions (represented physically by Mach lines). For more details about the mathematical treatment of the method the reader is directed to references [50-51]. The diverging section of the CSU wind tunnel consists of a linear expansion section that takes the fluid from sonic conditions at the throat up to the desired Ma=2.5 at the end of the expansion section. Once the flow reaches Ma=2.5 a flow straightening section is used to turn the flow back to be parallel with the nozzle centerline. The wall contour of the straightening section is turned exactly to match the flow turning angle at the point at which the waves meet the wall. The calculated nozzle contour produced by our custom-made code for our Mach 2.5 wind tunnel is shown in Figure 3.7 below.

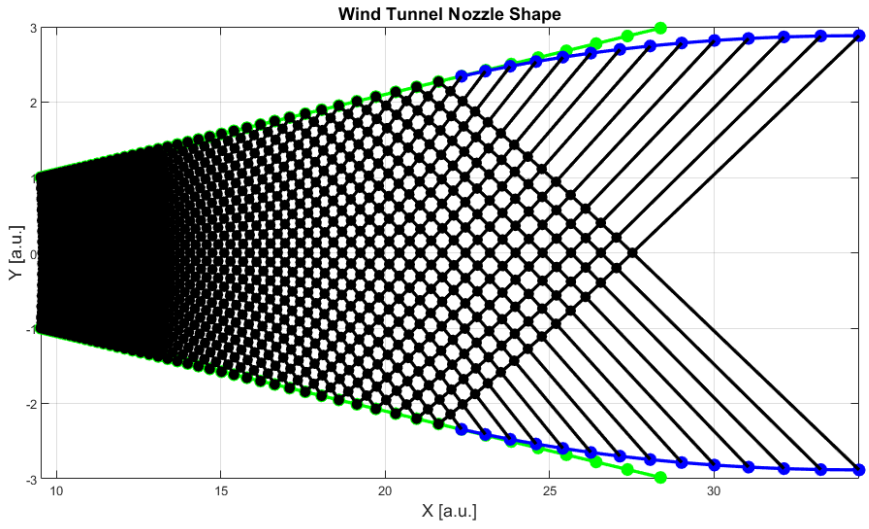

Figure 3.8: Mach 2.5 nozzle contour obtained via the Method Of Characteristics

3.2.3.2 Modeling Nozzle Startup

The behavior of supersonic flow within the converging-diverging nozzle is governed by several key physical principles: The conservation of mass, momentum, and energy govern the changes in flow properties through the nozzle. These principles are expressed through the continuity equation, momentum equation (Euler's equation), and energy equation.

The converging section reduces the cross-sectional area, causing the subsonic flow to accelerate as it moves towards the throat. According to the continuity equation, the decrease in area leads to an increase in velocity for subsonic flows, and results in a pressure drop. The throat is the narrowest part of the nozzle where the flow reaches sonic conditions (Mach 1). At this point, the flow velocity reaches the speed of sound. The mass flow rate through the nozzle is choked, meaning it cannot increase further even with an increase in upstream pressure.

The diverging section increases the cross-sectional area, allowing the flow to accelerate to supersonic speeds. For supersonic flow, the increase in area results in an increase in velocity and a decrease in pressure and temperature. This behavior is opposite to subsonic flow, where an increase in area would cause deceleration.

In supersonic flow, abrupt changes in flow properties are managed through shock waves and expansion waves. Shock waves cause a sudden increase in pressure and temperature while decreasing velocity, whereas expansion waves cause a smooth increase in velocity and decrease in pressure and temperature. The nozzle design aims to avoid normal shock waves in the diverging section to maintain efficiency. For supersonic flows, the area-velocity relationship is described by the area-Mach number relation, indicating that an increase in area leads to an increase in Mach number and velocity. This relationship is crucial for designing the diverging section to achieve the desired supersonic exit velocities.

As the wind tunnel starts up, air is evacuated downstream of the test section by the vacuum chamber at a finite rate. Shocks in the nozzle are inevitable during the transient tunnel startup process while the nozzle exit pressure is lowered by the vacuum chamber.

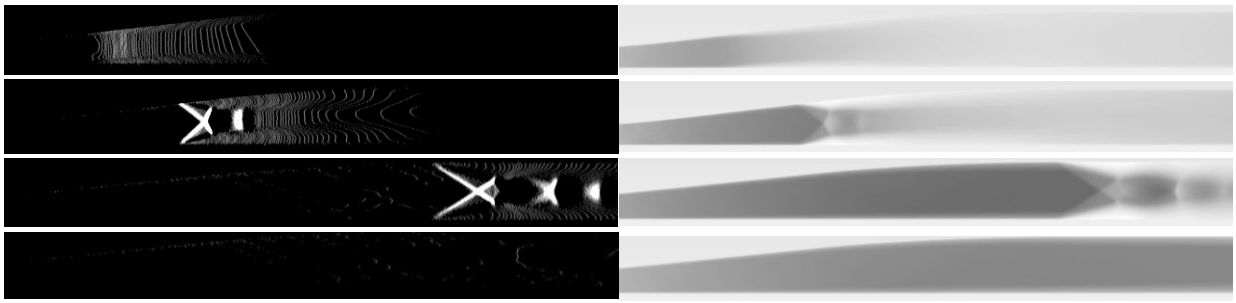

Figure 3.9: Nozzle synthetic schlieren (left) and density contours (right) at 75ms (top), 100ms, 125ms, and 150ms (bottom)

Optimal design of the subsonic contour was found by iteration of spline geometries in ANSYS fluent, following principles from Anderson [20]. Figure 3.9 only show very weak acoustic waves in the transonic region with a generally clean flow at the nozzle exit and into the test section. The fact that a symmetrical shock train develops during startup and steady-state boundary layers are relatively thin are indicators that this nozzle design is fit for wind tunnel use.

3.2.4 Test Section External Flow Modeling

We also wanted to better understand the impact of placing an aerodynamic object into the test section. As described by Pope & Czysz [27, 52], there are limitations to the size of the model that can be placed in the test section of a supersonic wind tunnel. In general, the presence of a model induces total head losses in the tunnel and can lead to flow unstart.

The flow around a wedge or strut in a supersonic wind tunnel exhibits several distinct features due to the high-speed, compressible nature of the flow. These features are characterized mainly by the formation of shock waves and expansion fans. When supersonic flow encounters the leading edge of a wedge or strut, it generates oblique shock waves. These shock waves form at an angle

relative to the flow direction, determined by the wedge angle and the Mach number of the incoming flow. Across the oblique shock wave, the flow undergoes a sudden increase in pressure, temperature, and density while experiencing a decrease in velocity. The flow remains supersonic but at a reduced Mach number.

If the wedge or strut has a trailing edge that causes the flow to turn away from itself, an expansion fan or Prandtl-Meyer expansion wave forms. This typically occurs at convex corners. The expansion fan consists of a series of infinitesimal expansion waves that cause the flow to accelerate, decreasing pressure, temperature, and density, while increasing the Mach number [20]. The change in flow properties through the expansion fan is described by the Prandtl-Meyer function, which relates the turning angle of the flow to the change in Mach number.

The interaction of shock waves with the boundary layer can lead to boundary layer separation. This occurs due to the adverse pressure gradient created by the shock wave. After separation, the flow may reattach downstream, forming a separation bubble. This interaction significantly affects the overall aerodynamic performance and must be carefully considered in design. At higher wedge angles or lower Mach numbers, the oblique shock wave may become detached, forming a normal shock wave ahead of the wedge. This leads to a significant increase in drag and pressure loss. Downstream of the wedge or strut, the flow may undergo reattachment and recompression, with additional shock waves forming as the flow readjusts. In a supersonic wind tunnel, the flow features around a wedge or strut can be observed and analyzed using various diagnostic tools.

To better size the wedge which will be used to perform initial calibration inside the tunnel, we also performed transient simulations (Figure 3.10). The main difference in the ANSYS Fluent setup is that the tunnel is set up as a variable geometry shock tube. For the starting procedure the tunnel pressure is held at 0.84 atm throughout and the dump tank beings at 0.001 atm. At t=0 an

artificial membrane that separates the two sides of the wind tunnel is removed (as in a shock tube simulation initialization) and the flow starts to develop inside the tunnel. Simulation results suggest that the tunnel can successfully start and reach steady-state flow conditions in 500 ms with a 10-degree, 6mm wedge inside a 40mm Mach 2.5 test section.

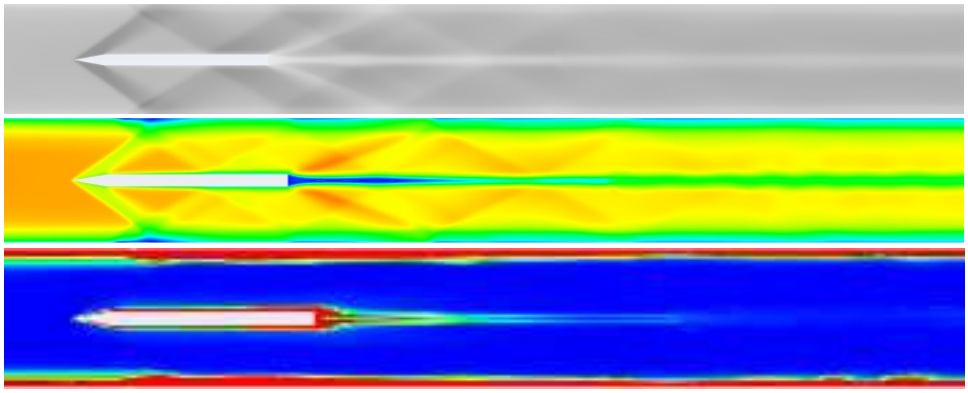

Figure 3.10: Test section and wedge density contour (top) Mach number contour (middle) and turbulent kinetic energy (bottom)

Shown in Figure 3.10 below is the synthetic schlieren image of the flow around the wedge once the tunnel reaches steady-state. By knowing the wedge angle and measuring the oblique shock wave angle form the synthetic schlieren image, one can calculate the Mach number at the tip of the wedge using the theta-beta-Mach relationship.

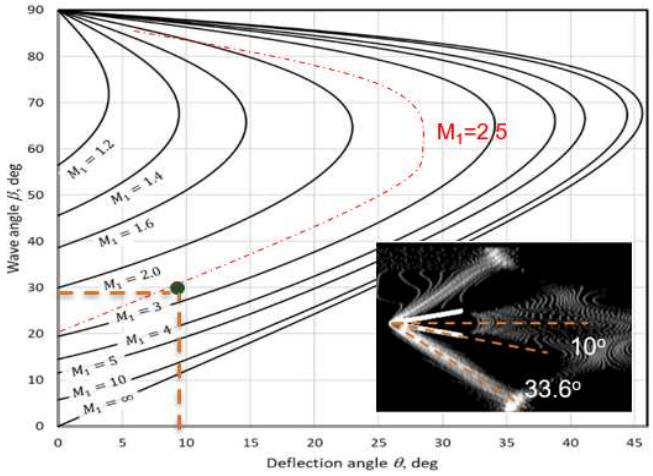

Figure 3.11: Theta-beta-Mach relationship and synthetic schlieren 10-degree wedge

3.2.5 Diffuser Modeling

Supersonic to subsonic diffusers play a crucial role in high-speed aerospace applications by efficiently decelerating high-speed airflow to subsonic speeds, ensuring stable and high-pressure conditions for engine operation. Their design involves careful management of shockwaves, flow transitions, and boundary layers to minimize losses and maximize performance. These devices are essential for the optimal functioning of jet engines, ramjets, and scramjets, enabling efficient and stable propulsion in high-speed flight regimes. In jet engines operating at supersonic speeds, the diffuser section of the inlet is responsible for decelerating the incoming airflow to subsonic speeds before it enters the compressor [20,27].

Properly designed diffusers minimize total pressure losses, which is crucial for maintaining high thermal efficiency. Boundary layer control, such as using bleed systems or boundary layer suction, helps to prevent flow separation and ensure a smooth transition from supersonic to subsonic flow. Managing the boundary layer and avoiding flow separation induced by shockwaves is critical for maintaining efficiency and reducing viscous effects. The temperature increases associated with decelerating supersonic flow must also be managed to prevent material fatigue and ensure long-term durability. Some diffusers incorporate variable geometry components, such as adjustable ramps or cowlings, to optimize performance across a range of operating conditions. Incorporating variable geometry can improve performance across different flight regimes but adds complexity to the design and operation.

In wind tunnels, diffusers play a crucial role in reducing power requirements by efficiently managing airflow and decreasing total pressure loss. This efficient energy management allows for longer, more sustained testing periods without overheating or wasted pressure differential, thereby extending the duration of tests and improving the overall efficiency and effectiveness of the wind

tunnel operations. Figures 3.12 & 3.13 illustrate the effectiveness of a simple converging-diverging diffuser at the end of our Mach 2.5 wind tunnel model by showing how the tunnel unstarts at a significantly higher backpressure, allowing for longer test times in our indraft wind tunnel. This diffuser geometry increases the unstart backpressure from 34 kPa to 44 kPa.

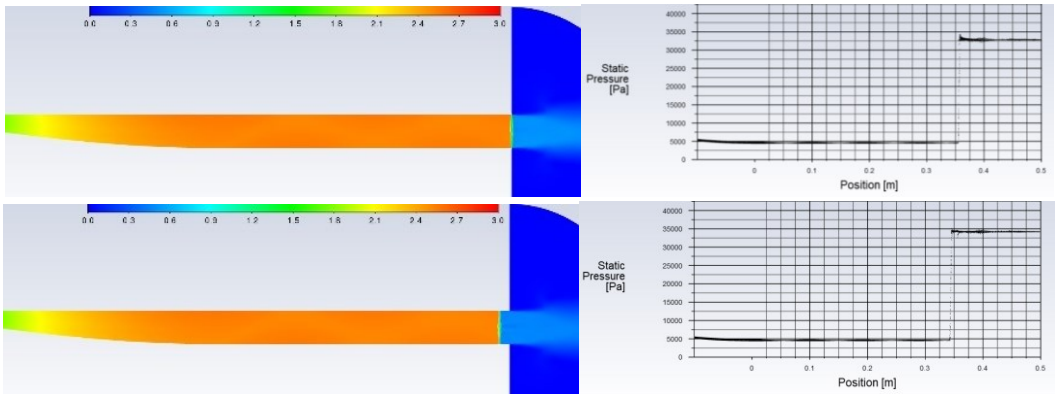

Figure 3.12: Wind tunnel transient simulation without diffuser Mach contours (left) and pressure plots (right) during steady-state operation (top) and during unstart (bottom)

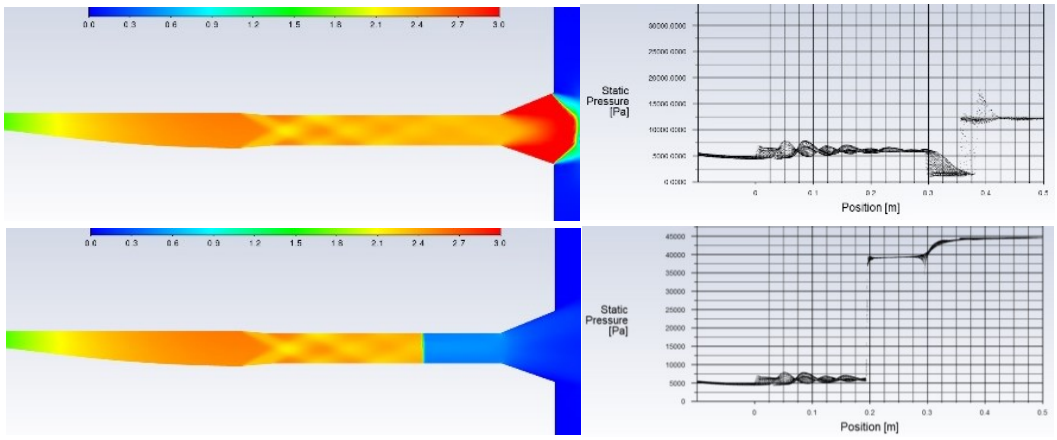

Figure 3.13: Wind tunnel transient simulation with diffuser Mach contours (left) and pressure plots (right) during steady-state operation (top) and during unstart (bottom)

Supersonic to subsonic diffusers are designed using several principles to achieve efficient flow deceleration and pressure recovery. By using a series of oblique shocks and area contraction, the diffuser can gradually decelerate the airflow while minimizing total pressure losses. The diffuser

often features a converging section followed by a diverging section. The converging section helps to decelerate the supersonic flow, while the diverging section aids in further deceleration and pressure recovery as the flow transitions to subsonic speeds. In some cases, a normal shock is used to abruptly decelerate the flow [20,27]. While this approach can result in higher pressure losses compared to oblique shocks, it is simpler and more compact.

While scramjets operate with supersonic combustion, during certain phases of flight or in hybrid engine designs, a diffuser may be used to decelerate flow to subsonic speeds in specific sections of the engine to create favorable ignition conditions.

3.2.6 Wind Tunnel Startup Model

An indraft wind tunnel operates by creating a low-pressure region downstream, which induces airflow through the test section. Before startup, the downstream chamber is evacuated to create a low-pressure region. The pressure upstream (atmospheric pressure) is higher than the pressure in the downstream chamber. A valve between the test section and the low-pressure chamber is opened (Figure 3.14 T=10ms). The pressure differential causes air to be drawn through the test section towards the low-pressure chamber (Figure 3.14 T=240 ms). As air flows into the low-pressure region, it accelerates through the converging-diverging nozzle, reaching supersonic speeds in the test section (Figure 3.14 T=660 ms).

Downstream pressure starts very low (evacuated) and gradually increases as the low-pressure chamber fills with air. The pressure rise must be managed to maintain stable supersonic flow. Indraft tunnels are relatively easy to start since the low-pressure region naturally draws air through the test section. Managing the downstream pressure rise is crucial for maintaining supersonic conditions, which may require continuous evacuation to sustain the pressure differential.

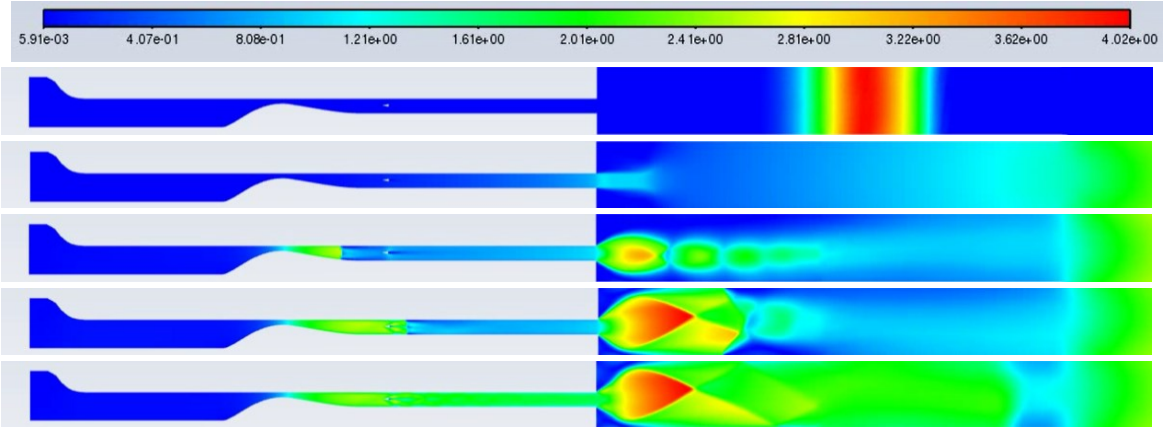

Figure 3.14: Indraft wind tunnel including a 6 mm 10-degree wedge Mach contours during startup at 10 ms (top), 240 ms, 660 ms, 1350 ms, and 2000 ms (bottom)

3.3 Mechanical Design

3.3.1 Inlet

The inlet of the indraft wind tunnel draws from the atmosphere and its role is to ensure that flow reaches the nozzle in a laminar fashion. The intake was designed to have a bell shape to avoid losses from boundary layer separation as the flow turns to enter the nozzle. The intake tube is constructed from the same structural steel tube as the test section and is a replaceable module to support future upgrades to the tunnel. Inside this section, several aluminum honeycomb structures are placed along its length to act as a flow straightener. A roof plate runs most of the length of the intake to enable the test size to be adjustable. A radius-diameter ratio for the bell mouth was determined which would generate minimal loss. After atmospheric air enters the bell-intake, a second neck-down occurs where the area is smoothly reduced to introduce the roof plate. After this, the flow enters the converging-diverging nozzle (Full flowpath can be seen in Figures 3.7 & 3.27). Each subsonic area neck-down is designed with continuous curvature to avoid flow separation.

Figure 3.15: Indraft wind tunnel bellmouth atmospheric intake

3.3.2 Nozzle

The converging-diverging nozzle was designed in several sections: subsonic, transonic/throat, and supersonic. The supersonic diverging contour was computed with a method of characteristics code and interpolated with a spline curve to generate the CAD profile for machining. The subsonic converging contour was designed using the best principal splines and iteratively tested in CFD to ensure there is no flow detachment resulting from the steep convergence. The transonic contour was designed to be parallel with the desired fluid velocity at the throat and connects the subsonic contour and supersonic expansion angle with continuous curvature. It was machined in-house with a 3D toolpath and ball mill over the surface of an aluminum billet. A picture of the linear asymmetric nozzle is shown in Figure 3.16.

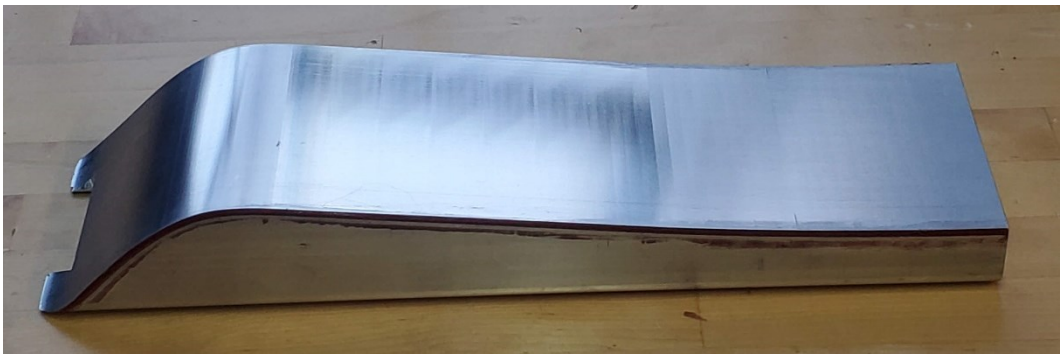

Figure 3.16: Aluminum billet nozzle for Mach 2.5 for 5.25” x 1.7” test size

3.3.3 Test Section

The wind tunnel test section was designed to interface with the upstream and downstream nozzle and diffuser/dump tank, enabling the study of the flow around the test setup. The inside of the test section features a roof plate and floor plate which are covered by a patter of 1/4"-20 through holes. These allow standard optical components to be mounted like an optical breadboard. It also allows for easy repositioning of objects in the test section. Figure x shows a slice of the test section with a sting and wedge installed. Figure x: Test Section Cut View Labeled Assembly Diagram A picture of the fully assembled final product is shown in Figure 3.17 below.

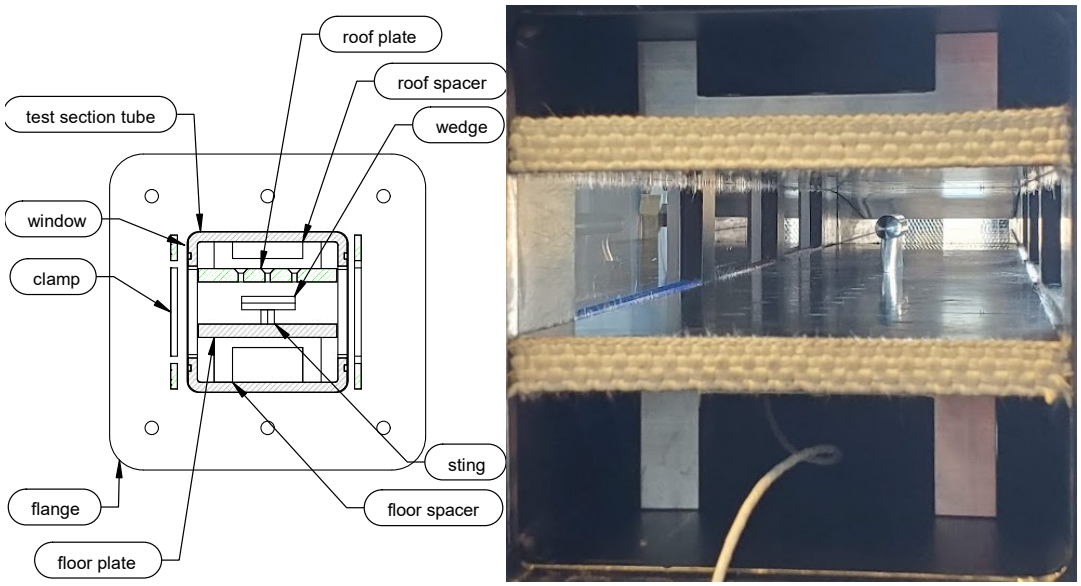

Figure 3.17: Wind tunnel section diagram with wedge installed and operational photo with pitot tube and gas seals installed

3.3.4 Vacuum Valve Actuator

In order to start the wind tunnel, the vacuum chamber must be exposed to the exit of the nozzle. It is advantageous to start the nozzle as fast as possible so that the maximum experimental time may be extracted from the volume and pressure of vacuum available in the tank. Figures 3.2 and

3.14 illustrate the theoretical maximum steady-state testing time and simulated startup sequence.

Many wind tunnels implement membranes or burst disks to suddenly expose the wind tunnel to a high-pressure differential, but the controlled destruction of these single-use pressure disks is wasteful and unreliable. In place of pressure disks, a fast-acting ball valve and actuator was produced to operate the indraft tunnel (Figure 3.18).

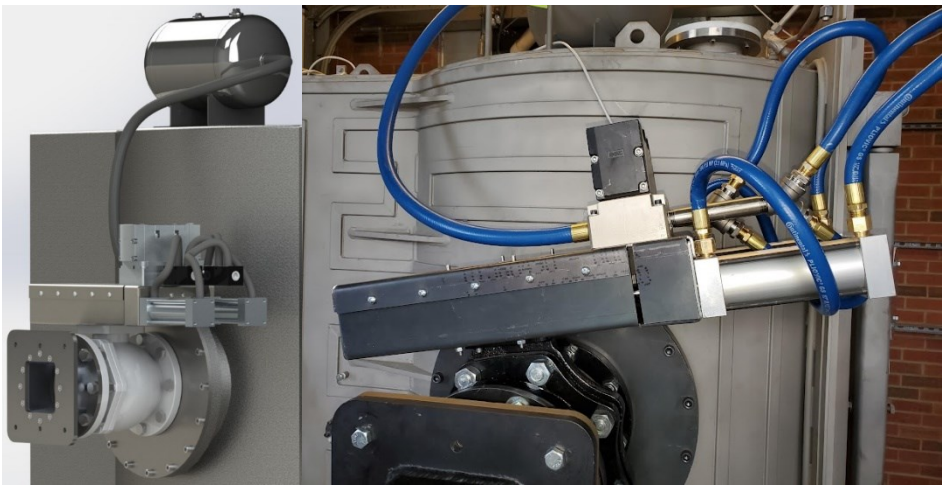

Figure 3.18: Exhaust system assembly rendering (left) and final product (right).

The exhaust system assembly consists of a common square flange, aluminum square-to-circular 3D aluminum transition, ball valve with actuator, and vacuum chamber adapter flange. The actuator is powered by shop compressed air regulated to 100-120psi in a buffer tank. The buffer tank stores air close to the piston solenoid where it is needed (Figure 3.19). A 5-way 2-position internal pilot pneumatic solenoid allows air from the buffer tank to either pressurize the close or open circuit of the actuator.

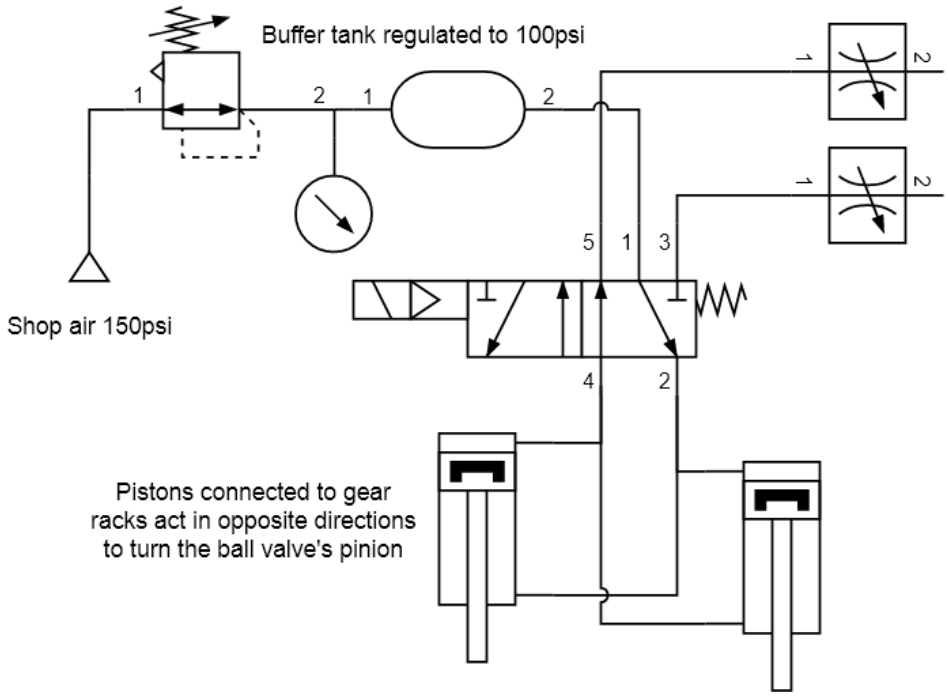

Figure 3.19: Vacuum ball valve actuator pneumatic diagram

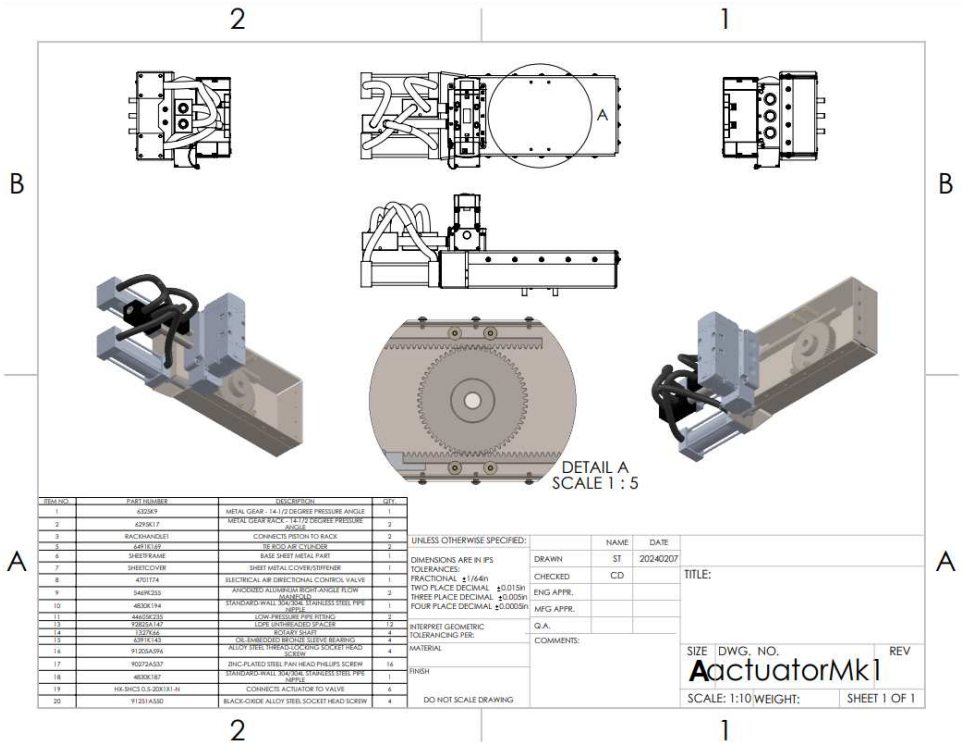

Figure 3.20: Valve actuator mechanical drawing

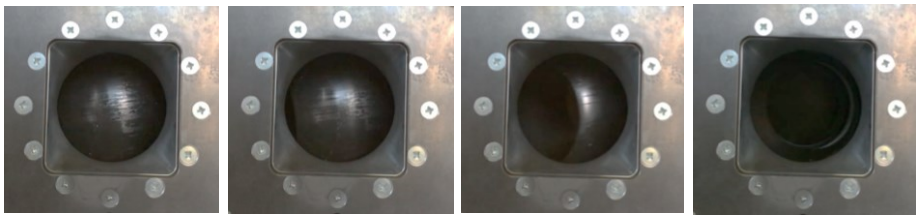

Figure 3.21: Valve opening over time. 0 ms (left), 200 ms 300 ms, 348 ms (right)

The ‘open’ and ‘closed’ sides of the pneumatic solenoid let air into opposite sides of two 2.5” pistons. These pistons push and pull on racks and a gear to turn the 6” ball valve 90 degrees left and right seal or open the vacuum chamber (Figure 3.20). The actuator was designed using constant-force analysis, which neglected acceleration forces. This analysis predicted a theoretical quickest opening time of 142 ms, but in practice required over 300 ms to completely open (Figure 3.21).

3.4 Vacuum System

Figure 3.22: Vacuum chamber state on delivery/donation

The vacuum dump tank used by the supersonic wind tunnel designed at CSU has a volume capacity of ~ 3.5 m^3. The tank has been previously used for plasma deposition applications and now had to be retrofitted for our wind tunnel. Several images of vacuum chamber are shown in

Figure 3.22. The pump and chamber arrived in a barebones state. The pump did not include any wiring or electrical control hardware. Because the pump and chamber are required for the feasibility of the project, configuring the pump (Figure 3.24) and sealing the chamber (Figure 3.22) were prioritized first. With the help of industry experts Greg Jackson and Colin Quinn, we were able to identify types of vacuum flanges and pump components needed for proper operation. We explored several options to seal the chamber with cost-benefit analysis. We considered: welding ports shut, purchasing many small plugs to seal the large flanges, and manufacturing our own blank plates for large flanges. We determined that welding smaller ports shut on larger plates would likely be cheaper than other options but leaves room for error in terms of voids, proper seal, and reusability. Purchasing many small, standard vacuum plugs for the ports in large flanges would be more expensive than just manufacturing new flanges ourselves and would add more failure points. We concluded that the best option to seal the chamber is to manufacture blank flanges ourselves.

Critically, the first step was to properly dimension the flanges needed to seal the tank. Finite element analysis was performed to meet safety factors on aluminum vacuum chamber flanges and optical windows. Stress and strain factors were determined for each component. This analysis ensured structural reliability and helped identify potential failure points to maintain system integrity. Finite element analysis was performed with the material and dimensions of our largest flange to verify that it will be strong and stiff enough. Our acceptable threshold of deflection is 0.050” according to industry expert Greg Jackson, but the simulated deflection was 0.025”. This confirmed that we may use the recommended 1” thick 6061 aluminum plate for the largest flange which experiences the highest load. The safety factor in terms of stress for this flange is above 3, which is acceptable for this application where forces are static.

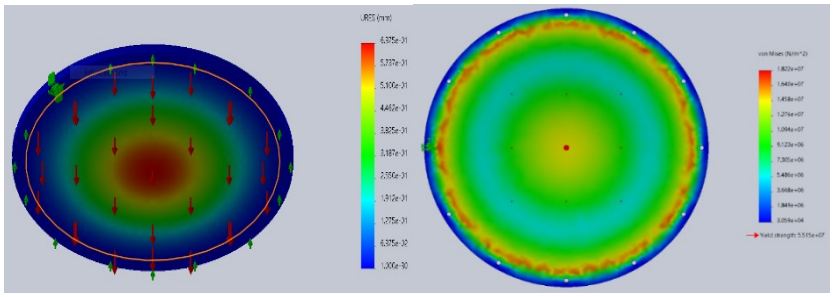

Figure 3.23: 42” x 1” vacuum flange stress analysis

A picture of the preliminary setup used to test the vacuum chamber is shown in Figure 3.24. A simple cooling loop cools the pump (Edwards QDP 40) while in operation. A vacuum tube connects the pump to the chamber with a valve inline. A pressure gauge mounted to the chamber indicates when the tunnel is at the desired starting pressure. Our vacuum pump was able to pump the chamber down from atmospheric pressure to 1 millibar in approximately 15 minutes.

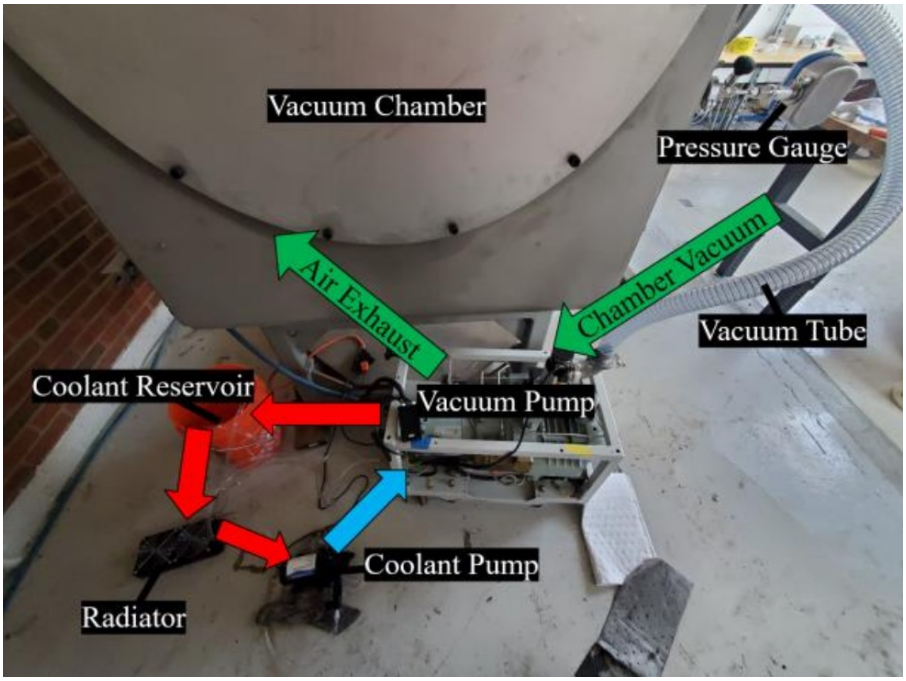

Figure 3.24: Vacuum system diagram

During the actual tunnel operation, the first step will be to pump down the chamber to 1 millibar with the shutoff valve between the pump and the test section closed. Once the valve is opened,

atmospheric air rushes through the tunnel filling the vacuum chamber. Supersonic testing is possible until the pressure in the chamber reaches a level that causes shock waves to appear in the converging-diverging nozzle. Ultimately, the run ends altogether when the pressure in the tank matches that of the ambient. In this configuration there is no need for a regulator valve, just shutoff.

3.5 Digital Controller

This digital controller (Figure 3.25) is designed for wind tunnel management, where an Arduino Uno R3 microcontroller serves as the central processing unit to manage various operations. The Arduino is programmed to send signals to different components of the wind tunnel system. These components include a coolant pump, vacuum valve, vacuum pump, and several triggering devices for external equipment.

Higher powered devices such as the 2.2 kw vacuum pump and coolant system are controlled by a series of relays. The Arduino's digital pins are connected ultra-low-power DC relays. These DC relays, when activated by the Arduino, control larger AC relays to power the high-voltage components.

In addition to managing the wind tunnel’s vacuum system, the Arduino also sends signals to trigger external devices. These include a high-speed camera, an oscilloscope, and a wind tunnel status gauge. The signals to these devices are typically sent through resistors to ensure proper current levels and to protect the Arduino from potential feedback.

A notable safety feature in this setup is the inclusion of a safety interlock button which controls the valve actuator solenoid. This ensures that the system can be safely shut down whenever the operator lets go of the interlock, and prevents accidental valve triggers when the operator is not in physical contact with the interlock.

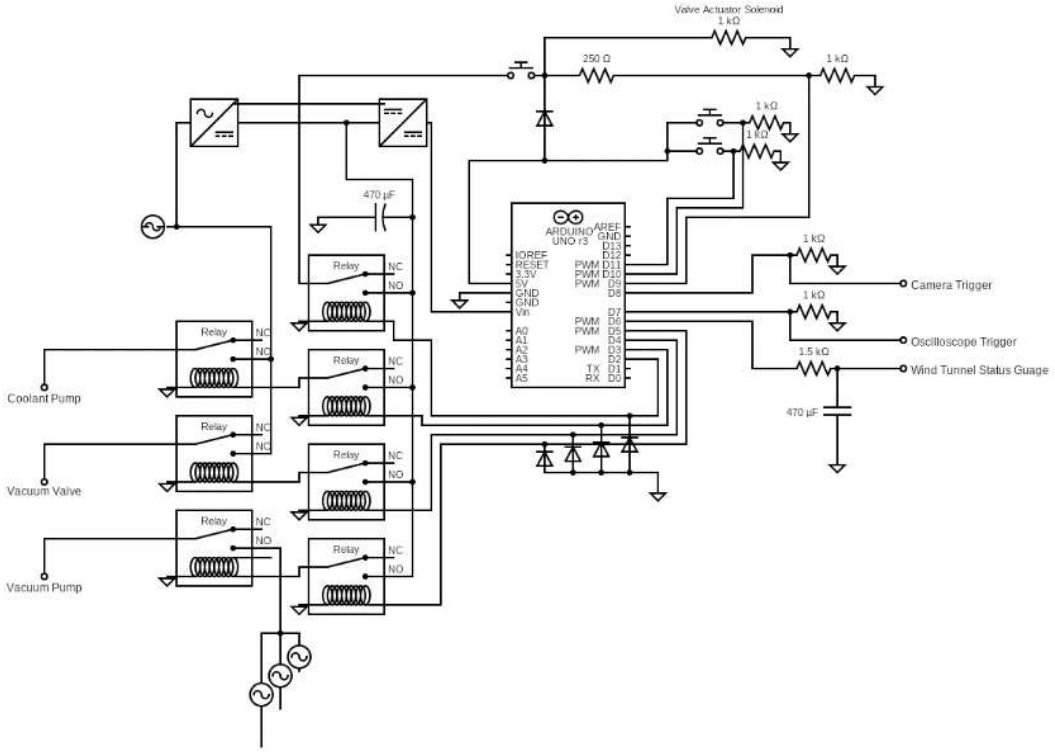

Figure 3.25: Wind tunnel digital control system circuit diagram

This digital controller setup exemplifies a robust method for interfacing a low-power microcontroller with high-power AC devices. By using DC relays to drive AC relays, the system leverages the control and programmability of the Arduino while safely managing high-power operations. The inclusion of external device triggers and safety interlocks ensures that the wind tunnel can operate efficiently and safely, making it an effective solution for controlling complex systems with varied requirements.

3.6 Schlieren Imaging

Schlieren images will be used regularly to analyze flows inside the tunnel; they provide a clear view of shock wave angles, expansion fans, and boundary layer interactions. To create a Schlieren image, a point light source is directed through a collimating lens to produce a collimated light

beam. The beam is then passed through the test section, where it interacts with the density variations in the airflow. The light beam is then refocused using another curved mirror or lens and directed onto a knife-edge. These density variations in the wind tunnel cause small refraction angles in the light beam, deflecting light around the blade, which produces the Schlieren effect. The resulting image appears as a series of bright and dark bands, which correspond to regions of high to low density in the test section.

The CSU supersonic wind tunnel schlieren setup is pictured in Figure 3.26. It features a z-type folded design, where mirrors fold the focusing light path onto itself in efforts to reduce the space requirement. The primary mirrors used for light collimation an focusing are 203 mm in diameter with an 800 mm focal length. Secondary and tertiary 3-4" elliptical and 1" circular planar mirrors used for folding the focusing beam into the high-speed camera or point source generator.

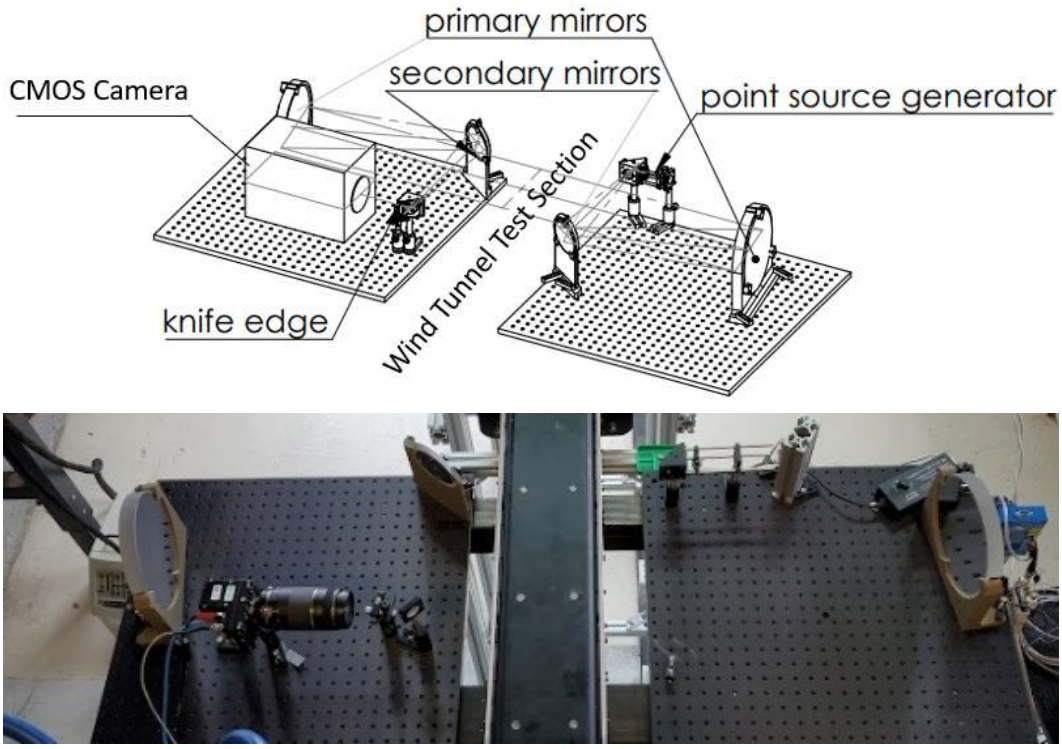

Figure 3.26: Schlieren optical Solidworks layout (top) and implementation (bottom)

Synthetic schlieren imaging was used in supersonic flow simulations for comparison with experimental results. These synthetically generated images will be compared to real Schlieren images from the test section. The image processing involves using the density gradient of a computational domain to produce a synthetic image of the flow field. This is done by taking the difference in the density between two points in the flow along a certain axis determined by the orientation of the knife-edge, and then using this to calculate the density gradient. The density gradient is then used to produce a synthetic schlieren image of the flow field.

3.7 Assembled Wind Tunnel

The wind tunnel is fully modular. Common square flanges were designed which allows modules to be connected to form the entire wind tunnel. Current modules include the intake/plenum, converging- diverging nozzle, test section, valve connection, and vacuum connection.

Steel parts were manufactured in collaboration with the Powerhouse machine shop. The test section, block off plates, and connection flanges were machined from mild steel, and test articles, window clamps, and sting were milled from aluminum stock. O-rings were made from standard sized chord stock, silica windows will be custom cut in the future, while currently 1/8 acrylic sheet was is used for the test section windows.

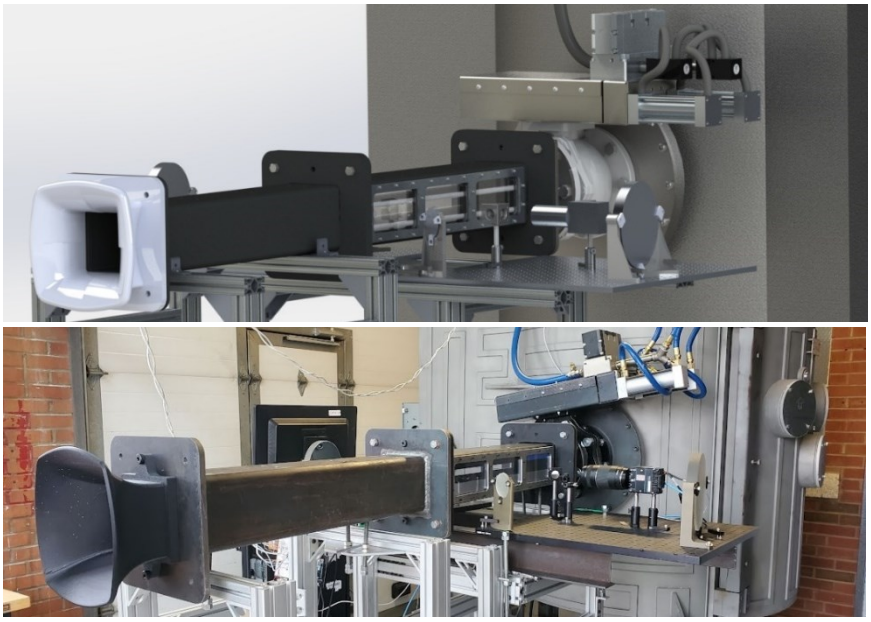

Figure 3.27: Wind tunnel Solidworks rendering (top) and manufactured product (bottom)

Chapter 4 Results

Three different experiments were designed to validate the flow Mach number inside the wind tunnel. Schlieren was set up to measure oblique and bow shockwaves from a wedge and a spherical blunt body rake along the wind tunnel test section (Figures 4.2 & 4.2). In addition, a high accuracy pressure transducer probe measured stagnation pressure seen in Figure 4.3 (Kulite XCS-190S-15A). These experiments are meant to deduce the Mach number and demonstrate the facility's capability to collect high-fidelity spatial flow data.

4.1 Wedge Experiments

Figure 4.1 shows the oblique shock wave pattern formed around the wedge. The determination of the Mach number involves measuring the oblique shock angle from a wedge of known angle. This method relies on trigonometric relationships to infer Mach number:

$$\tan\theta = 2\cot\beta \frac{{Ma_1}^2 \sin^2\beta - 1}{{Ma_1}^2(\gamma + \cos 2\beta) + 2} \tag{4.1}$$

Several frames of the schlieren video were used to obtain averages and standard deviation. The beta angle was determined using an edge finder MATLAB algorithm and the wedge was precisely machined to a 10° angle 1/8" thick and 0.5" wide.

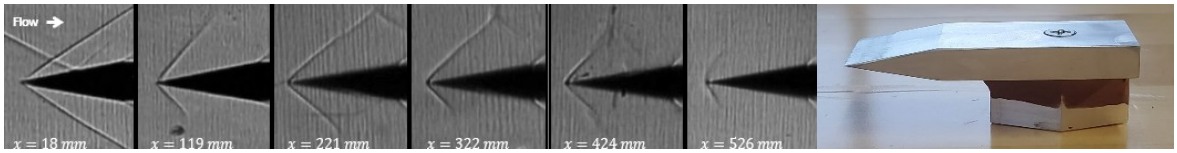

Figure 4.1: Oblique shockwave Schlieren images along test section (left) and aluminum 10-degree wedge (right)

4.2 Sphere Experiments

Figure 18 shows the bow shockwave standoff from a sphere. The standoff distance is the point where the shockwave created by the object reaches equilibrium with the oncoming flow. Determining this distance requires Schlieren interferometry, with uncertainty stemming from variations in flow conditions, shockwave patterns, and image spatial resolution. Distance measurements were completed by interpolation between pixel brightness to find the best approximation for the normal shock to body distance. Frames of Schlieren video during steady-state operation were used to obtain averages and standard deviation. The following equation is then used to find the incident Mach number using the radius of the blunt body sphere [53-54].

$$\frac{D_{BS}}{D_{OB}} = 1 + 1.1\frac{(\gamma-1)Ma^2+2}{(\gamma+1)Ma^2} \tag{4.2}$$

D_{BS} and D_{OB} represent distance to the bow shock and the distance to the spherical blunt from the body origin.

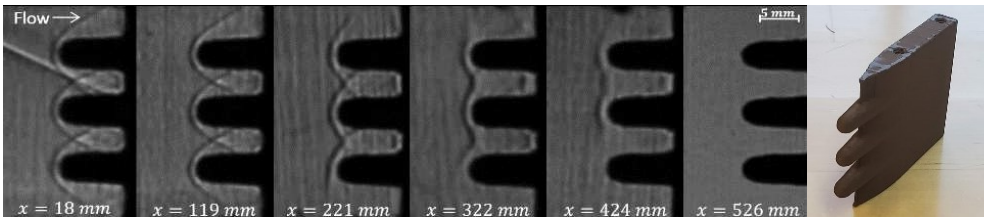

Figure 4.2: Bow shockwave Schlieren images along test section (left) and spherical-tipped blunt body rake (right)

4.3 Stagnation Pressure Experiments

Stagnation pressure measurements constitute the third validation method. By assessing the change in stagnation pressure from a normal shockwave, one can infer Mach number using Eq. 4.3. These measurements have inherent uncertainties due to sensor precision, calibration, and variation over the steady state period.

$$\frac{p_{02}}{p_{01}} = \left(\frac{(\gamma+1)Ma_1^2}{(\gamma-1)Ma_1^2+2}\right)^{\frac{\gamma}{\gamma-1}} \left(\frac{\gamma+1}{2\gamma Ma_1^2-(\gamma-1)}\right)^{\frac{1}{\gamma-1}} \tag{4.3}$$

To get an accurate picture of the average and variation, a digital oscilloscope (BitScope) was used to quantify the stagnation pressure. Data was collected at a rate of 6.85 kHz for 841 ms with a resolution of 250 Pa. It is crucial to note that this measurement technique assumes the flow is isentropic before the normal shock formation in front of the probe (i.e., there are no losses of total pressure prior to the normal shock anchored in front of the probe). Total pressure losses before the

nozzle ultimately adds a positive offset to the Mach number computed from pitot pressure data. As our schlieren results illustrated above, several weak oblique shocks are formed in the tunnel, particularly around the windows. Therefore, pressure measurements downstream are less reliable and they diverge from the optical measurements noted. Nonetheless, the pressure probe (Figure 4.3) can be reliably used to measure the radial profile of the Mach number at the nozzle exit. These results, presented in Figure 4.4-left, show that the Mach number remains relatively constant across the test section.

Figure 4.3: Stagnation pressure probe installed in the test section

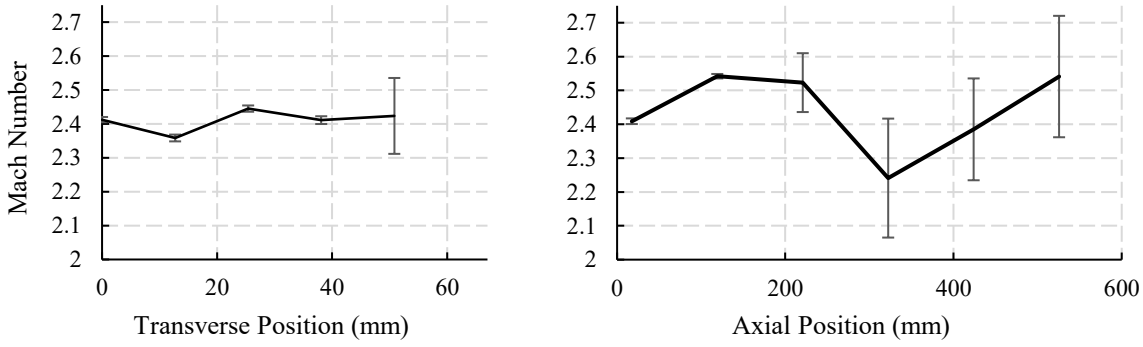

Figure 4.4: Computed Mach number from stagnation pressure in the transverse (left), and axial (right) directions. Average and standard deviation were computed using 3000 samples

4.4 Mach Number Plot Results

The results from these optical measurements of Mach number are reported in Figure 4.5. The measurements confirm that the Mach number at the nozzle exit is very close to design conditions (actual Mach = 2.42). As the wedge and the spherical probe rake are translated downstream, we note a decrease in Mach number such that, at the exit of the test section, Ma ~ 1.5. The disparities between a sphere and a wedge (Figure 4.5) underscore the necessity of considering geometry-specific behaviors in aerodynamic measurements. Aerodynamic influences, which may alter the axial Mach number results between the wedge and sphere, may include shocks generated by the nozzle gas seals perpendicular to the flow at the nozzle exit (Figure 4.1 & 4.2 at 18 mm position), boundary layer flow in the rectangular step between the test-section's steel wall and windows. To validate these results, calculations were completed using Fanno flow to estimate Mach number along the length of the test section. The best correlating parameters are a friction factor of 2.5E-3 and Mach number of 2.42 at the test section entrance.

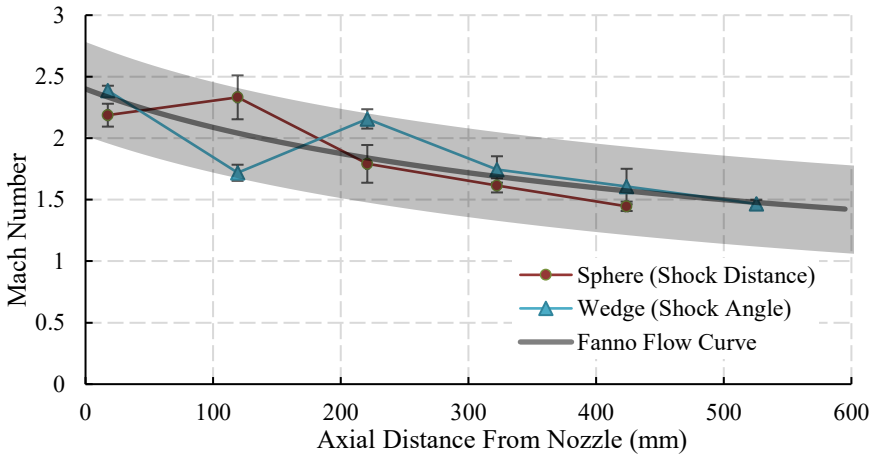

Figure 4.5: Calculated Mach numbers along the test section based on 2 optical experimental methods compared with Fanno flow theory. 10 samples with each probe were used at each position for an average and standard deviation

4.5 Repeatability

The repeatability of the wind tunnel was measured with the stagnation pressure probe. The wind tunnel was run several times and the similarity between the data was compared to determine the natural difference in tests (Figure 4.6). For this test, data was collected at 400 Hz for 4 seconds. Data collection starts at the same time as the command is given to open the main vacuum valve. During the first half second, the valve actuator pilot receives power, then the main solenoid opens, pressuring the actuator pistons. After enough pressure to overcome friction has built in the pistons, the ball valve turns to allow air into the vacuum chamber (See section 3.3.4). The wind tunnel and probe start up, as shown by the sharp change in stagnation pressure ratio, indicating loss over shockwaves.

The average start time after the commanded test start is 499 ms with a standard deviation of 29 ms over 6 tests. The average Mach number of the steady state duration for these 3 tests (Figure 4.6) was 2.41 with a standard deviation of 0.0079. The average test duration was 1307 ms with a standard deviation of 21 ms. This observed steady-state supersonic test duration changes depending on the location of the probe. Duration decreases in time and increases in variation along the length of the test section and close to the walls due to drag.

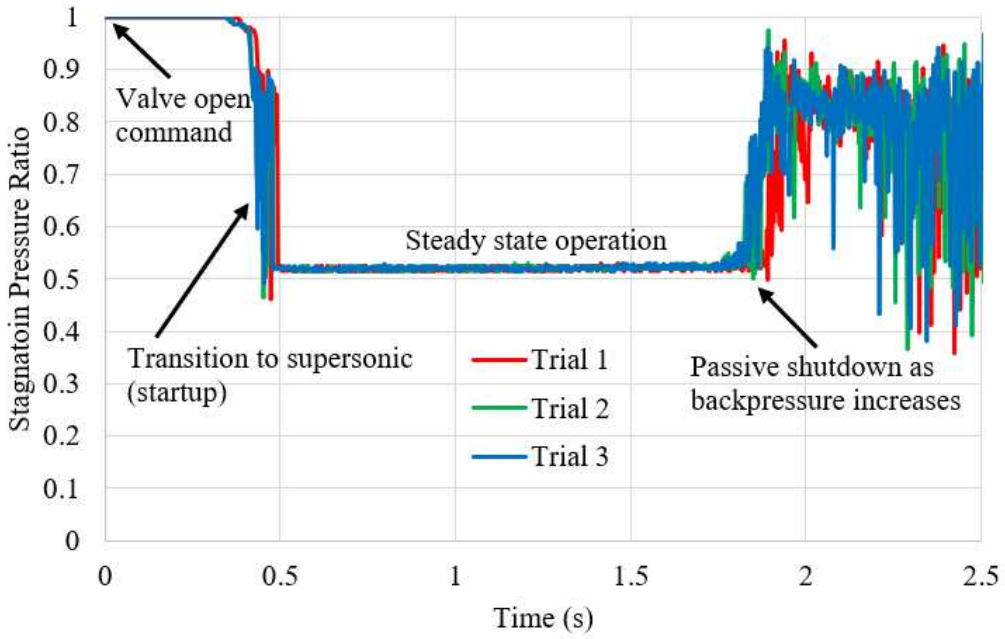

Figure 4.6: Stagnation pressure ratio before and after the nozzle for 3 representative tests measured directly after the nozzle in the center of the test section

Chapter 5 Conclusion

5.1 Summary

A supersonic wind tunnel was built at Colorado State University to study supersonic flows in relation to scramjet propulsion. This manuscript presented the design, integration, and validation of the wind tunnel. Currently, the tunnel operates at Mach 2.4, with a test section size of 1.57" x 5.25" over a period of ~1.3 seconds. The tunnel was equipped with a folded z-type schlieren system to study the effect of shock waves inside the test section. Preliminary testing has focused on Mach number determination inside the test section via three methods: wedge, spherical blunt body, and pressure probe measurements. The first two methods rely on schlieren visualization of the shock waves to extract the flow Mach number. The third method infers the Mach number by measuring

the total pressure losses across the normal shock that forms in front of the pressure probe. Experimental results obtained with all three methods agreed and demonstrated the tunnel's capability to provide high-fidelity spatial and temporal flow data, crucial for accurate scramjet testing.

5.2 Future Work

The CSU wind tunnel offers a versatile, cost-effective platform for studying scramjet engine physics. The tunnel's modular test section, diagnostic capabilities, and modularity position it as a valuable tool for research in supersonic combustion and hypersonic flight technologies. A high-enthalpy heating module is under development to increase the temperature and pressure upstream of the nozzle. Additionally, work is underway on Mach 5 and Mach 7.5 nozzles. This will increase the temperatures and velocity in the test section to allow for future combustion studies and more accurate replication of scramjet flight conditions (Figure 3.5).

Also of interest is the study of laser ignition inside a flame holder and the use of plasma as a method of active control of flame stabilization and/or boundary layer control inside a scramjet combustor. Fuel will be injected into the test section through the mounting system, and ignition will be attempted with an optical spark. The test section may be reconfigured to house flameholder geometries or diverging plates as in some scramjet combustors. Laser diagnostics, such as Kr two-photon laser-induced fluorescence (Kr TALIF), laser Rayleigh scattering, and laser spark velocimetry will ultimately be installed to better characterize the flow inside the tunnel.

Bibliography

[1] “Pratt & Whitney J58 Turbojet Engine (SR-71),” *www.sr71blackbird.org*. https://www.sr71blackbird.org/engine.php

[2] K. Austin and B. Mechanical, “Evolutionary Design of Robust Flight Control for a Hypersonic Aircraft,” 2002. Accessed: Jun. 15, 2024. [Online]. Available: https://gdtk.uqcloud.net/pdfs/kevin-austin-phd-thesis-june-2002.pdf

[3] “Why it’s time to reach for full reusability,” *Aerospace America*, May 01, 2021. https://aerospaceamerica.aiaa.org/departments/why-its-time-to-reach-for-full-reusability/

[4] B. W. Augenstein and E. D. Harris, "The National Aerospace Plane (NASP): Development Issues for the Follow-on Vehicle, Executive Summary," RAND Corporation, Project Air Force, Santa Monica, CA, 1993.

[5] R. Ricketts, T. Noll, W. Whitlow, and L. Huttsell, “NASA Technical Memorandum 107728 AN OVERVIEW OF AEROELASTICITY STUDIES FOR THE NATIONAL AERO-SPACE PLANE,” 1993. Accessed: Jun. 15, 2024. [Online]. Available: https://ntrs.nasa.gov/api/citations/19930014233/downloads/19930014233.pdf

[6] N. Hass, M. Smart, and A. Paull, “3 th AIAA/CIRA International Space Planes and Hypersonic Systems and Technologies Conference Flight Data Analysis of HyShot 2.” Available: https://ntrs.nasa.gov/api/citations/20050215040/downloads/20050215040.pdf

[7] L. A. Marshall, G. P. Corpening, and R. Sherrill, “A Chief Engineer’s View of the NASA X-43A Scramjet Flight Test,” *AIAA/CIRA 13th International Space Planes and Hypersonics Systems and Technologies Conference*, Jan. 2005, doi: https://doi.org/10.2514/6.2005-3332.

[8] “X-51A Waverider,” *U.S. Air Force*. https://www.af.mil/About-Us/Fact-Sheets/Display/Article/104467/x-51a-waverider/

[9] M. Christopher, M. Rondeau, L. Col, T. Jorris, and Director, “SFTE 44th International / SETP Southwest Flight Test Symposium, X-51A SCRAMJET DEMONSTRATOR PROGRAM: WAVERIDER GROUND AND FLIGHT TEST,” 2013. Accessed: Jun. 15, 2024. [Online]. Available: https://apps.dtic.mil/sti/tr/pdf/ADA593742.pdf

[10] J. Lane, “Design Processes and Criteria for the X-51A Flight Vehicle Airframe.” Accessed: Jun. 15, 2024. [Online]. Available: https://www.sto.nato.int/publications/STO%20Meeting%20Proceedings/RTO-MP-AVT-145/MP-AVT-145-1.7.pdf

[11] “Tackling the Extreme Challenges of Air-Breathing Hypersonic Vehicle Design, Technology, and Flight Design, Technology, and Flight.” Accessed: Jun. 15, 2024. [Online]. Available: http://aero-comlab.stanford.edu/jameson/aj80th/bowcutt.pdf

[12] *Darpa.mil*, 2022. https://www.darpa.mil/news-events/2022-07-18

[13] DARPA, "Hypersonic Air-breathing Weapon Concept (HAWC)," [Online]. Available: https://www.darpa.mil/program/hypersonic-air-breathing-weapon-concept.

[15] *Darpa.mil*, 2023. https://www.darpa.mil/news-events/2023-01-30

[16] *Darpa.mil*, 2022. https://www.darpa.mil/news-events/2021-09-27

[18] S. Caldwell, “State-of-the-Art of Small Spacecraft Technology,” *NASA*, Jun. 25, 2020. https://www.nasa.gov/smallsat-institute/sst-soa-2020

[19] “X-43A Hyper-X - NASA,” *NASA*. https://www.nasa.gov/reference/x-43a/

[20] John David Anderson, *Modern compressible flow : with historical perspective*. New York: Mcgraw-Hill, 1990.

[21] McGann, B., Lee, T., Ombrello, T., Carter, C. D., Hammack, S. D., and Do, H. “Inlet Distortion Effects on Fuel Distribution and Ignition in Scramjet Cavity Flameholder.” Journal of Propulsion and Power, Vol. 35, No. 3, 2019, pp. 601–613. https://doi.org/10.2514/1.B37204.

[22] Yang, L., An, B., Liang, J., Li, X., and Wang, Z. “Dual-Pulse Laser Ignition of Ethylene-Air Mixtures in a Supersonic Combustor.” *Optics Express*, Vol. 26, No. 7, 2018, p. 7911. https://doi.org/10.1364/oe.26.007911.

[23] Brieschenk, S., Kleine, H., and O’Byrne, S. “Laser Ignition of Hypersonic Air–Hydrogen Flow.” Shock Waves, Vol. 23, No. 5, 2013, pp. 439–452. https://doi.org/10.1007/s00193-013-0447-6.

[24] Brieschenk, S., O’Byrne, S., and Kleine, H. “Laser-Induced Plasma Ignition Studies in a Model Scramjet Engine.” Combustion and Flame, Vol. 160, No. 1, 2013, pp. 145–148. https://doi.org/10.1016/j.combustflame.2012.08.011.

[25] Dumitrache, C., Butte, C., and Yalin, A. “Resonant Dual-Pulse Laser Ignition Technique Based on Oxygen REMPI Pre-Ionization.” Scientific Reports, Vol. 10, No. 1, 2020, pp. 1–11. https://doi.org/10.1038/s41598-020-76968-5.

[26] Butte, C., Dumitrache, C., and Yalin, A. P. Dual-Pulse Laser Ignition Using Oxygen REMPI Preionization. 2019.

[27] Pope, A., and Goin, K. High Speed Wind Tunnel Testing. John Wiley & Sons, Inc., London, 1965.

[28] NASA Glenn Research Center, "8x6 Supersonic Wind Tunnel," [Online]. Available: https://www1.grc.nasa.gov/facilities/8x6/.

[29] NASA Glenn Research Center, "10x10 Supersonic Wind Tunnel," [Online]. Available: https://www1.grc.nasa.gov/facilities/10x10/.

[30] NASA, "9- by 7-Foot Supersonic Wind Tunnel Facility," [Online]. Available: https://www.nasa.gov/directorates/armd/aetc/9-by-7-foot-supersonic-wind-tunnel-facility/.

[31] Oehlschlaeger, M. A., Davidson, D. F., and Hanson, R. K. “High-Temperature Ethane and

Propane Decomposition." Proceedings of the Combustion Institute, Vol. 30, No. 1, 2005, pp. 1119–1126. https://doi.org/10.1016/j.proci.2004.07.032.

[32] Ludweig, H. "Tube Wind Tunnel, a Special Type of Blowdown Tunnel." Tech. rep. North Atlantic Treaty Organization.

[33] Kimmel, R. L., Borg, M., Jewell, J. S., Lam, K. Y., Bowersox, R., Srinivasan, R., Fuchs, S., and Mooney, T. "AFRL Ludwieg Tube Initial Performance." AIAA SciTech Forum - 55th AIAA Aerospace Sciences Meeting, No. January, 2017. https://doi.org/10.2514/6.2017-0102.

[34] Schrijer, F. F. J., and Bannink, W. J. "Description and Flow Assessment of the Delft Hypersonic Ludwieg Tube." *Journal of Spacecraft and Rockets*, Vol. 47, No. 1, 2010, pp. 125–133. https://doi.org/10.2514/1.40773.

[35] Cummings, R. M., and McLaughlin, T. E. "Hypersonic Ludwieg Tube Design and Future Usage at the US Air Force Academy." 50th AIAA Aerospace Sciences Meeting Including the New Horizons Forum and Aerospace Exposition, No. January, 2012, pp. 1–15. https://doi.org/10.2514/6.2012-734.

[36] Saenz, L., Vergeer, L., Frankel, J., and Shu, F. Characterization of the Mach 5 Shock Tunnel at New Mexico State University. 2023.

[37] NASA Glenn Research Center, "Hypersonic Tunnel Facility," [Online]. Available: https://www1.grc.nasa.gov/facilities/htf/.

[38] Johnson, D. K. "The Design and Validation of the New Supersonic Indraft Tube Wind Tunnel at Cal Poly San Luis Obispo." Aiaa Aviation 2020 Forum, Vol. 1 PartF, 2020, pp. 1–35. https://doi.org/10.2514/6.2020-3109.

[39] Segal, C. "A Unique, Mach 6 Enthalpy, Non-Vitiated Facility for Hypersonic Aerodynamics Research." *17th AIAA International Space Planes and Hypersonic Systems and Technologies*

Conference 2011, No. April, 2011. https://doi.org/10.2514/6.2011-2278.

[40] Gray Kidd, F., Narayanaswamy, V., Danehy, P. M., Inman, J. A., Bathel, B. F., Cabell, K. F., Hass, N. E., Capriotti, D. P., Drozda, T. G., and Johansen, C. T. "Characterization of the NASA Langley Arc Heated Scramjet Test Facility Using NO PLIF." AIAA AVIATION 2014 - 30th AIAA Aerodynamic Measurement Technology and Ground Testing Conference, 2014, pp. 1–17. https://doi.org/10.2514/6.2014-2652.

[41] Guy, R. W., and Torrcnce, M. G. "Operating Characteristics of the Langley Mach 7 Scramjet Test Facility." NASA TM-81929, 1981.

[42] Thomas, S. R., and Guy, R. W. "Expanded Operational Capabilities of A Langley Mach 7 Scramjet Test Facility." NASA Technical Paper 2186, 1983.

[43] R. G. Morgan, A. Paull, and R. J. Stalker, "Shock Tunnel Studies of Scramjet Phenomena," NASA Contractor Report, NASA-CR-201693, Apr. 1997. [Online]. Available: https://ntrs.nasa.gov/api/citations/19970022388/downloads/19970022388.pdf.

[44] Hannemann, K., Martinez Schramm, J., Wagner, A., Friedl, D., and Ponchio Camillo, G. "The High Enthalpy Shock Tunnel Göttingen of the German Aerospace Center (DLR)." *Journal of large-scale research facilities JLSRF*, Vol. 4, 2018, pp. 1–14. https://doi.org/10.17815/jlsrf-4-168.

[45] Johansen, C. T., McRae, C. D., Danehy, P. M., Gallo, E. C. A., Cantu, L. M. L., Magnotti, G., Cutler, A. D., Rockwell, R. D., Goyne, C. P., and McDaniel, J. C. "OH PLIF Visualization of the UVa Supersonic Combustion Experiment: Configuration A." *Journal of Visualization*, Vol. 17, No. 2, 2014, pp. 131–141. https://doi.org/10.1007/s12650-014-0197-2.

[46] Andrews, Philip, Philip Lax, Skye Elliott, Alexander Firsov, and Sergey Leonov. 2022. "Flow Characterization at Heated Air Supersonic Facility SBR-50" Fluids 7, no. 5: 168. https://doi.org/10.3390/fluids7050168

[47] NASA, "8-Foot High Temperature Tunnel (HTT)," Fact Sheet, 2016. [Online]. Available: https://www.nasa.gov/wp-content/uploads/2016/01/8ft_htt_fact_sheet_508.pdf?emrc=1c5b90.

[48] Plans and Programs Directorate, "AFRL successfully completes GDE-2 testing," *Wright-Patterson Air Force Base News*, Dec. 12, 2006. [Online]. Available: https://www.wpafb.af.mil/News/Article-Display/Article/401453/afrl-successfully-completes-gde-2-testing/.

[49] Baccarella, D., Liu, Q., Passaro, A., Lee, T., and Do, H. "Development and Testing of the ACT-1 Experimental Facility for Hypersonic Combustion Research." *Measurement Science and Technology*, Vol. 27, No. 4, 2016. https://doi.org/10.1088/0957-0233/27/4/045902.

[50] Liepmann, H. W., and Roshko, A. Elements of Gasdynamics. John Wiley & Sons, Inc., New York, 1957.

[51] Ascher H. Shapiro. The Dynamics and Thermodynamics of Compressible Fluid Flow. The Ronald Press Company, New York, 1953.

[52] P. A. Czysz, "Correlation of Wind Tunnel Blockage Data," Technical Documentary Report, No. ASD-TDR-63-230, Wright-Patterson Air Force Base, OH, Apr. 1963.

[53] Farris, M. H., and Russell, C. T. "Determining the Standoff Distance of the Bow Shock: Mach Number Dependence and Use of Models." *Journal of Geophysical Research: Space Physics*, Vol. 99, No. A9, 1994, pp. 17681–17689. https://doi.org/10.1029/94JA01020.

[54] I. A. Bedarev, A. V. Fedorov, V. M. Fomin, "Numerical analysis of the flow around a system of bodies behind the shock wave", *Combustion, Explosion and Shock Waves*, Vol. 48, No. 4, 2012, pp. 446–454. https://doi.org/10.1134/S0010508212040119.

Appendix

Appendix A Rayleigh Flow

Rayleigh flow refers to the study of one-dimensional compressible flow with heat addition or removal without any work being done on or by the flow. It is named after Lord Rayleigh, who first analyzed such flows. This type of flow is important in understanding the behavior of fluids in various engineering applications, including propulsion systems like ramjets and scramjets.

In Rayleigh flow, the key assumption is that the flow is steady, one-dimensional, and adiabatic, but with heat addition or removal. The flow parameters such as pressure, density, temperature, and velocity change due to the heat added or removed.

In Rayleigh flow, choking occurs when the flow velocity reaches the speed of sound (Mach 1) due to heat addition. At the choking point, the flow cannot accommodate further increases in heat addition without causing a reduction in mass flow rate.

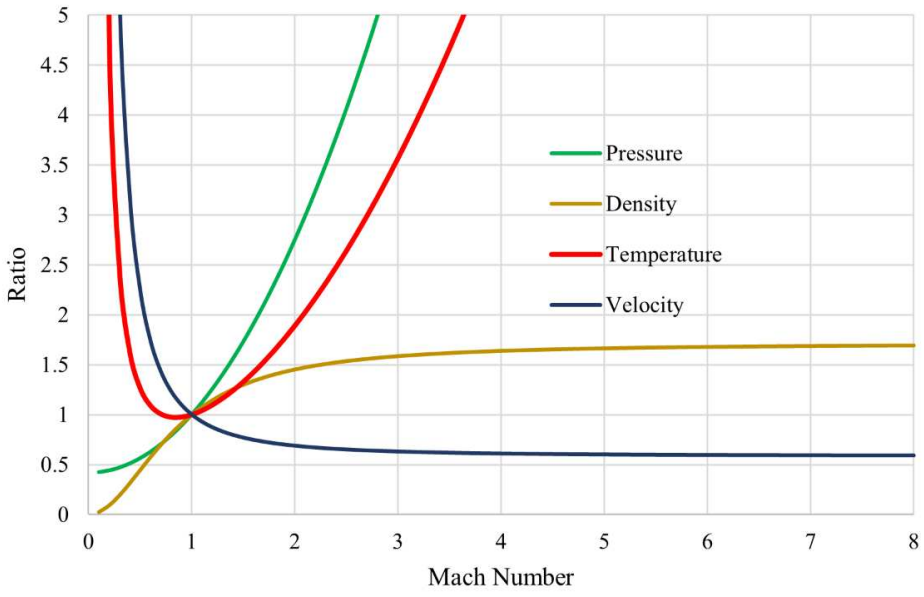

Figure A.1: Rayleigh flow choking ratios for pressure, density, temperature, and velocity

At different Mach numbers, these ratios describe how the temperatures change relative to their choking conditions. At higher Mach numbers, the heat addition causes larger changes in the stagnation temperature due to the higher energy of the flow.

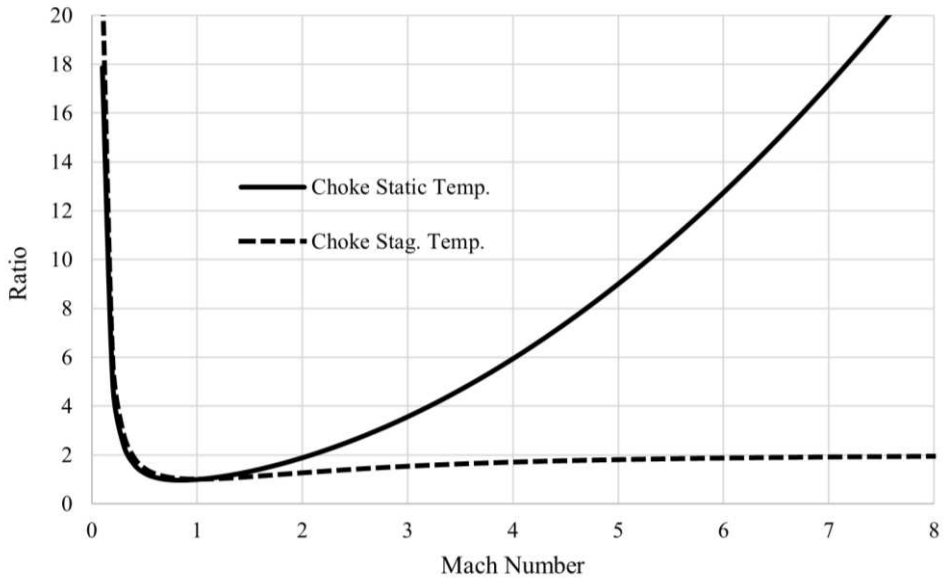

Figure A.2: Rayleigh flow choking ratios for static and stagnation temperature against Mach number

The Rayleigh temperature is significant in the context of ramjets and scramjets because it represents the temperature at which the flow has maximum entropy for a given heat addition. This is critical for designing efficient propulsion systems.

Ramjets operate at subsonic to supersonic speeds where the airflow is decelerated to subsonic speeds in the combustor. The heat addition process in the combustor can be analyzed using Rayleigh flow principles to ensure optimal performance and avoid choking.

Scramjets operate at hypersonic speeds where the airflow remains supersonic throughout the engine. Rayleigh flow analysis helps in understanding the impact of heat addition on the supersonic flow, ensuring that the combustor is designed to handle high-speed, high-temperature conditions without causing flow separation or choking.

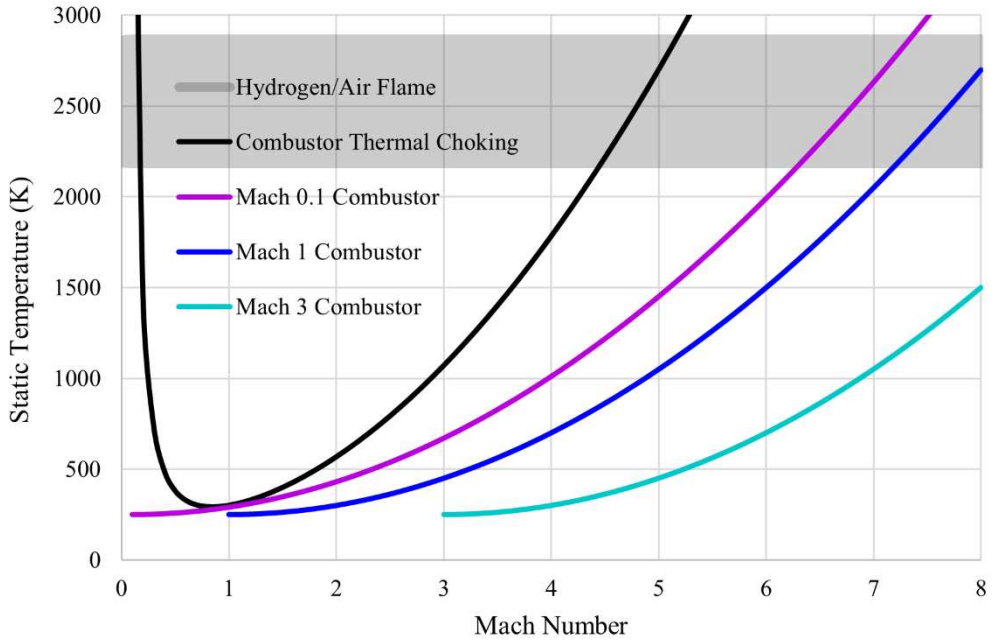

Figure A.3: Rayleigh flow thermal choking static temperature against Mach number for different combustion Mach numbers

In turbojets, thermal choking can occur in the afterburner, a component where additional fuel is burned downstream of the main combustion chamber to produce extra thrust. In the afterburner, the temperature of the exhaust gases is increased by burning additional fuel. This heat addition increases the specific volume of the gases. The increase in specific volume leads to an increase in the flow velocity. If the velocity reaches the speed of sound, the flow becomes choked. When the flow is choked, any further addition of heat (fuel) cannot increase the mass flow rate. Instead, it only increases the temperature and pressure downstream of the choking point.

Ramjets rely on the high-speed intake air being decelerated to subsonic speeds in the combustor, where fuel is added and burned. As the high-speed intake air is decelerated and fuel is burned, the temperature of the flow increases. With increasing heat addition, the flow velocity can approach the speed of sound at the narrowest point of the combustor or the exit. If the temperature increase is sufficient to cause the flow to reach Mach 1, the flow becomes choked.

Scramjets operate at hypersonic speeds where the airflow remains supersonic throughout the engine. In scramjets, combustion occurs in a supersonic flow. The heat addition in the combustor increases the temperature and pressure of the flow. By definition, the design must ensure that the flow remains supersonic throughout the engine. If the heat addition causes the flow velocity to reach Mach 1 locally, it can lead to a normal shock wave forming, which decelerates the flow to subsonic speeds, causing a loss of efficiency and potentially engine failure. Scramjets are designed to avoid thermal choking by carefully managing the amount of heat added and the pressure distribution within the combustor to maintain supersonic flow conditions.

Appendix B Wind Tunnel Operation

The operation of the wind tunnel is often independent of the type of experiment being run due to its modular nature. To run different experiments, the only changes in the process are to how the inside of the wind tunnel is configured with hardware, the arrangement of the optical table, sensor connections, and electrical timing triggers. Figure B.1 below illustrates the process of performing an experiment with the wind tunnel.

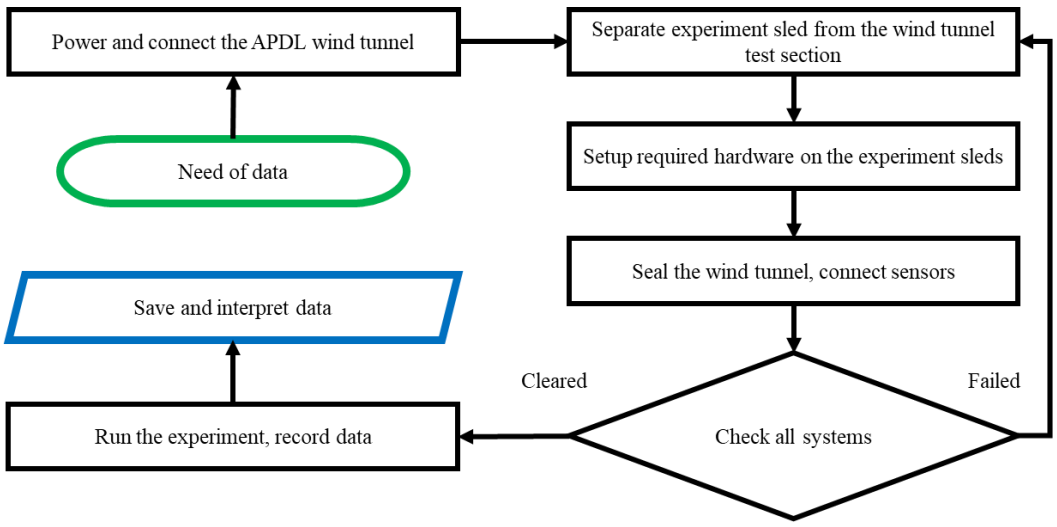

Figure B.1: Wind tunnel operation flowchart

General Setup

1) Power on the wind tunnel AC panel
2) Plug in the Arduino board USB cable
3) Check for good actuator regular pressure ~ 115 psi
4) Check that vacuum chamber door is closed

Software Setup

1) Open Arduino IDE and test code
2) Enter “enable vacuum” into the Arduino IDE console to turn on the vacuum system

Test Section Setup

1) If using the rear test section bulkhead (as in a pitot probe experiment), split the test section and diffuser modules, otherwise split the test section and intake modules

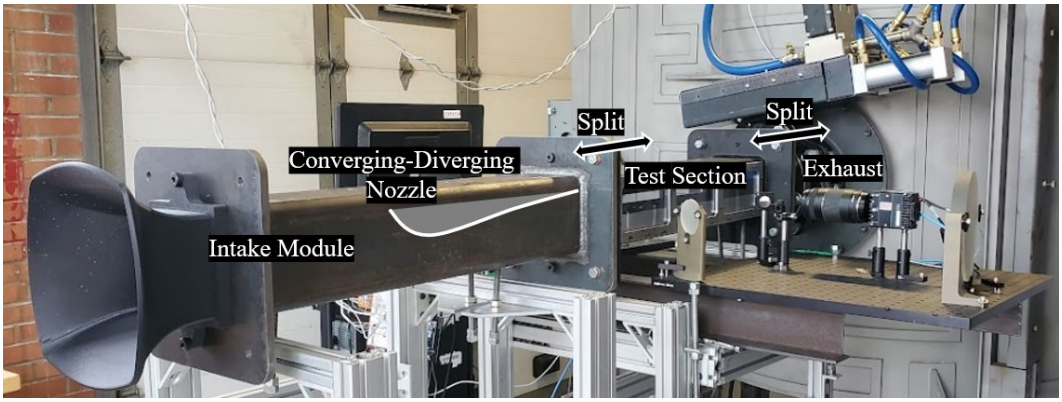

Figure B.2: Wind tunnel module splitting diagram

a. While using the rear test section bulkhead, raise the 3 test section jacks before splitting modules
b. Use a 3/4 inch socket to remove the 4 square flange nuts
c. Slide the modules apart on the railcars

i. Apply force on the module and the railcart at the same time
ii. Be aware of wired connections from the test cart to the computer cart or other test equipment while sliding modules apart

2) Unscrew & remove 4 #8 screws from an experiment sled, slide it out
3) Prepare the experiment sled on the bench including test article placement, wiring, strain relief, tubing, standoff sizing, and front/side seal inspection. See Pitot Tube Setup below as one example of an experiment setup procedure.
4) Undo steps 2 and 1, re-inserting shoulder bolts first where applicable, and use screw jacks to line up module flanges
5) Inspect the intake/test section mating flange pressure by holding a light to the seals, looking for even compression and a flush transition

Pitot Tube Setup

1) Configure the pitot probe in the desired configuration with blunt or sharp tip and off-set or perpendicular pieces
2) With a test sled on the bench, feed the wires through a mounting point, and use front and back screws to secure the probe
3) Connect the pitot probe passthrough wires to the main cable, match colors
4) Do Test Section Setup steps 3-5, also lining up the cable with a bulkhead
5) Connect the pitot tube cable to the signal conditioner
6) Connect the BitScope to the control PC via USB
7) Modify the Arduino code to trigger the oscilloscope capture at the required time
8) Open BitScope DSO, refer to software experiment setups saved in the BitScope folder

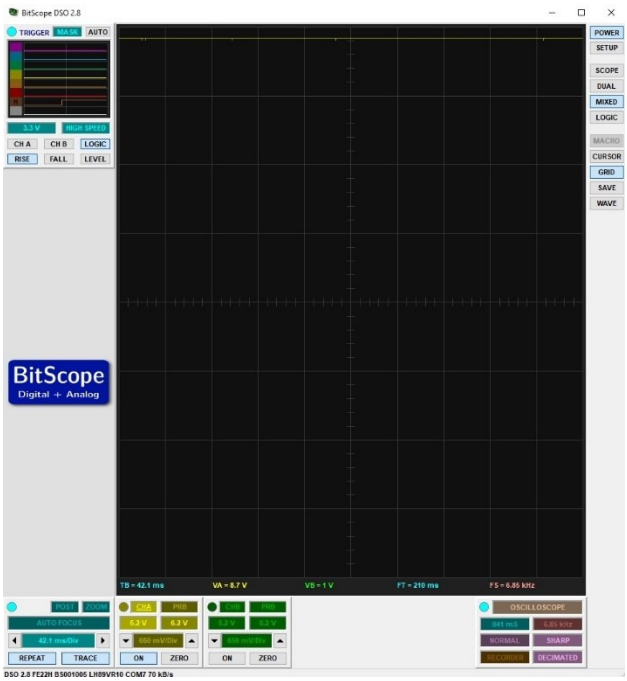

Figure B.3: BitScope DSO selected options for stagnation pressure probe data collection

Schlieren Setup

1) Plug in camera power, ethernet, and auxiliary signal cables
2) Power on the schlieren light source
3) Modify the Arduino code to trigger the camera capture at the required time
4) Open the PCC software, align the camera using the kinematic table and railcart
5) Choose the desired camera settings, press capture, then trigger using Arduino control or with the PCC trigger button

Running an Experiment

1) Wait for a ready signal on the Arduino serial monitor or on the wind tunnel needle gauge
2) Hold the red button on the AC panel for at least the duration of the experiment defined by the Arduino code
3) Review and save data from relevant sources

Notes

- Vacuum system cooling fans may be left plugged in at any time, but AC & DC electronics should be unplugged before work on the AC box or around the pneumatic actuator
- The vacuum pump typical hot side coolant temperature is ~45 C
- The vacuum chamber should be left at low pressure when shutting the system down, this prevents the vacuum chamber door from swinging open and contaminants entering
- Follow this procedure to adjust shims on the flowpath plates
    - Mount both test section sleds, use bore gauge or blocks to measure the distance across the plates for squareness and proper test section size
    - Adjust test section shims as needed, the test section plates are used as reference for the intake nozzle and plate
    - Loosely tighten the nozzle and plate dovetail mounts
    - Lightly tighten the test section to intake flange
    - Tighten the nozzle and plate dovetail mounts
    - Tighten the test section to intake flange,
    - Inspect the intake/test section mating flange pressure by looking for even compression, look through the front of the intake and through each side of the test section
    - Measure the transition between intake and test section plates with a straightedge and shims
    - Adjust shims if necessary and repeat

Appendix C Digital Controller Logic

An Arduino Nano is used to operate the wind tunnel. It is responsible for interpreting written commands, monitoring the vacuum system, operating the main pneumatic valve, and sending signals to experimental hardware. The code may be referenced in Figure C.2, and a flowchart diagram of the code can be seen in Figure C.1 below.

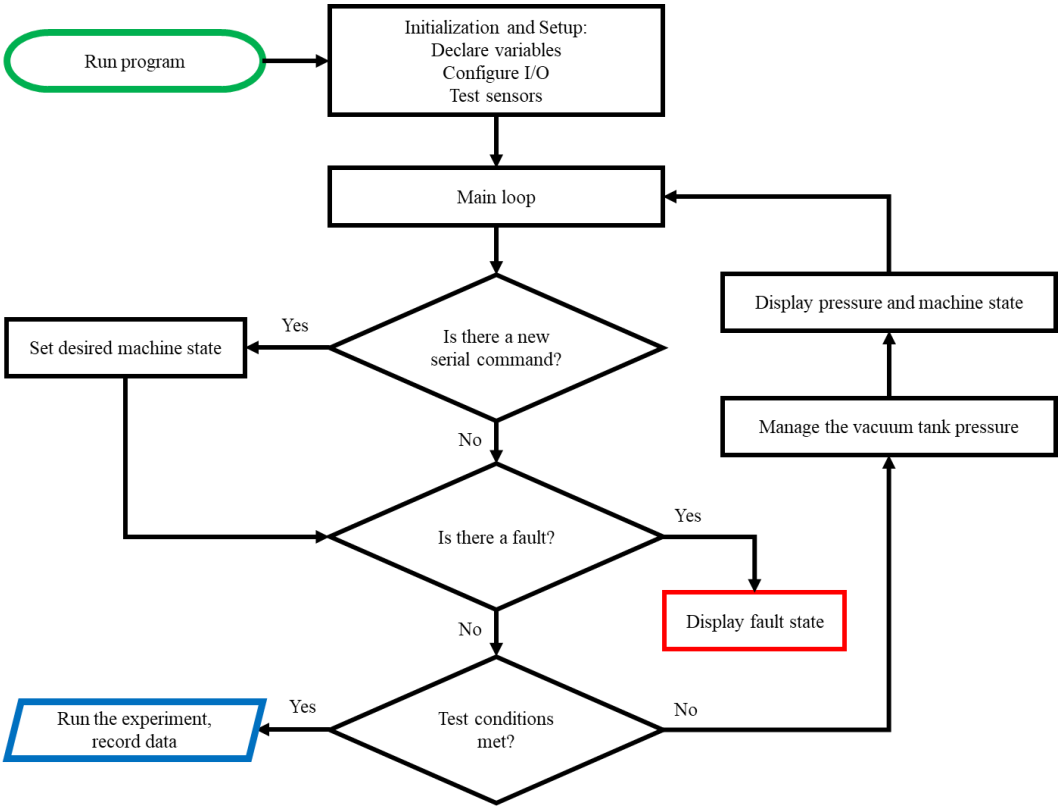

Figure C.1: Arduino microcontroller code diagram

```
int pressInt = 0;
float tankPressureTarget = 0.03; //mbar
bool pumpState = 0;
bool faultState = 0;
bool readyState = 0;
bool vacSysRun = 0;
const float Pmin = 0.0;  //for tank pressure transducer
const float Pmax = 1.03421359;
const float VminComp = 0.5;
const float VmaxComp = 4.5;
const int RangeMin = 115;
const int RangeMax = 226;  //for tank pressure map to indicate needle out of
255
float pressureBar = 0.0;
```

```
int temp = 0;

void setup();
void loop();
void vacPumpON();
void vacPumpOFF();
void indicateNeedle(String zone);
int measureTankPressure();
void setup() {
  Serial.begin(9600);
  // Initialize the digital pins as outputs
  pinMode(2, OUTPUT);  // valve actuator relays
  pinMode(3, OUTPUT);  // coolant pump relays
  pinMode(4, OUTPUT);  // vacuum pump relays
  pinMode(5, OUTPUT);  // vacuum valve relay
  pinMode(6, OUTPUT);  // indicator needle PWM
  pinMode(7, OUTPUT);  // oscillopscope trigger
  pinMode(8, OUTPUT);  // camera trigger
  pinMode(9, INPUT);   // TEST RUN RED BUTTON
  // write all pins low for now
  digitalWrite(2, LOW);
  digitalWrite(3, LOW);
  digitalWrite(4, LOW);
  digitalWrite(5, LOW);
  digitalWrite(7, LOW);
  digitalWrite(8, LOW);
  measureTankPressure();
}

void loop() {
  // Depending on your requirements, you might want to run this sequence con-
tinuously.
  // If you only need it to run once, keep the loop empty.
  delay(1000);
  //measure voltage from pressure transducer on the vacuum tank, throws an
error if it is physically imppossible
  if (pressInt > 922 || pressInt < 102) {
    Serial.println("!! TANK PRESSURE TRANDUCER FAULT DETECTED !!");
    faultState = 1;
  }
  // Process the input string if it's complete: (commands)
  if (Serial.available() > 0) {
    // Read the incoming string until newline character is detected:
    String command = Serial.readStringUntil('\n');
    // Remove any trailing newline or carriage return characters:
    command.trim();
    // Compare the command with "enable vacuum":
    if (command == "override start vacuum") {
      // If the command matches, run the function:
      vacPumpON();
    } else if (command == "override stop vacuum") {
      vacPumpOFF();
    } else if (command == "enable vacuum") { //automatically pump down the
chamber to the target pressure, will hold there, will set the state to ready
      pumpState = 1;
    } else if (command == "sweep gauge") { //debugging for calibrating the
gauge
```

```
      delay(3000);
      analogWrite(6, RangeMin);
      delay(2000);
      analogWrite(6, RangeMax);
      delay(2000);
      analogWrite(6, 187);
      delay(2000);
    } else if (command == "test triggers") {  //useful for testing camera
triggering, laser triggering, any external signal
      Serial.println("Triggering.");
      digitalWrite(7, HIGH); //oscope
      digitalWrite(8, HIGH); //camera
      delay(1000);
      digitalWrite(7, LOW);
      digitalWrite(8, LOW);
      Serial.println("Triggered.");
    } else if (command == "disable vacuum") { //disables the automatic vacuum
keeping/readiness
      vacPumpOFF();
      pumpState = 0;
    } else if (command == "override start cooling") { //for the vacuum cool-
ing system, used when running the pump for many hours, give it some extra
cooling during a break
      digitalWrite(3, HIGH);
      Serial.println("Coolant pump on.");
    } else if (command == "override stop cooling") { //for the vacuum cooling
system
      digitalWrite(3, LOW);
      Serial.println("Coolant pump off.");
    } else {
      // Optional: Handle unrecognized commands or add more commands here
      Serial.println("Command not recognized.");
    }
  }
  if (faultState) {  //disables the controller if a condition is met, valve
actuator, vacuum system, or the Ptransducer
    indicateNeedle("fault");
    Serial.println("~~~FAULT STATE~~~");
    delay(10000);
  } else if (pumpState) { //this is where we automatically control the vacuum
tank pressure
    Serial.print("Vacuum tank at ");
    Serial.print(pressureBar, 3);
    Serial.print(" bar."); //display the pressure to the serial monitor,
could also use the serial plotter
    Serial.println();
    if (pressureBar > tankPressureTarget) { //if the pump isnt running and
pressure is too high, turn it in
      if (!vacSysRun){
        vacPumpON();
      }
    }
    if (pressureBar <= tankPressureTarget) { //if the pressure target has
been reached, tiurn the pump off and go tho the ready state
      if (vacSysRun){
        vacPumpOFF();
      }
```

```
      pumpState = 0;
      readyState = 1;
      Serial.println("State READY, vacuum achieved. ");
    }
    indicateNeedle("pressure"); //function calculates and sends voltage to
the needle indicator
  } else if (readyState) { //keep pressure in the tank at the target, has a
leak threshold (4 millibar works well)
    if (pressureBar > (tankPressureTarget + 0.004)) {
      Serial.println("Pressure target lost, re-evactuating...");
      pumpState = 1; //turn the pump state on, then the above code runs
      readyState = 0;
    } else {
      indicateNeedle("ready");
    }

  }
  if (readyState & !digitalRead(9)) { //this code runs when the state is
ready and we hold the red button
    Serial.println("Running...");
    digitalWrite(2, HIGH);//give command to open valve (usually delay of 500-
700ms before tunnel starts)
    //the following code is what you write to design a test, synchronizes
everything with the red button


    digitalWrite(8, HIGH);//trigger camera
    digitalWrite(7, HIGH);//trigger oscope

    // temp = 1;
    // while (temp < 20){
    //   digitalWrite(8, HIGH);//fire laser trigger
    //   delay(1);
    //   digitalWrite(8, LOW);//untrigger laser
    //   delay(149);
    //   temp = temp + 1;
    // }
    delay(4000);
    digitalWrite(8, HIGH);//trigger camera
    digitalWrite(7, HIGH);//trigger oscope

    //keep the following code constant (end of the test code)
    digitalWrite(2, LOW);
    delay(1000);
    measureTankPressure();
    if (pressureBar < (tankPressureTarget + 0.001)) { //prevents the test
code from running multiple times upon a sticky valve actuation
      Serial.println("!! VALVE FAULT DETECTED !!");
      faultState = 1;
    }else{
      readyState = 0;
      pumpState = 1;
    }
  }
  measureTankPressure(); //function looks at the voltage from the tank pres-
sure transducer, and calculates the bars from voltage
}
```

```
void vacPumpON() {
  measureTankPressure();
  int temp = pressInt;
  Serial.println("Attempting to evacuate the chamber...");
  digitalWrite(3, HIGH);
  Serial.println("Coolant pump on.");
  digitalWrite(4, HIGH);
  Serial.println("Vacuum pump on.");//this gives time for the vacuum pump to
reach a low pressure in the line
  delay(1000);  // Wait 1 second
  digitalWrite(5, HIGH);
  Serial.println("Vacuum valve open.");//solenoid opens
  Serial.println("Testing seal...");
  delay(2000); // wait 2 secs
  measureTankPressure();
  if(temp < pressInt){
    Serial.println("!! VACUUM PUMP SYSTEM FAULT DETECTED!!");
    vacPumpOFF();
    faultState = 1;
  }else{
    Serial.println("Good chamber pressure...");
    Serial.println("Vacuum system running...");
    vacSysRun = 1;
  }
}

void vacPumpOFF() {
  Serial.println("Attemping to seal vacuuum chamber...");
  digitalWrite(5, LOW);
  Serial.println("Vacuum valve closed.");
  delay(500);  // Wait 0.5 seconds, makes sure that we don't rotate the pump
backwards
  digitalWrite(4, LOW);
  Serial.println("Vacuum pump off.");
  delay(100);  // Wait 0.1 seconds
  digitalWrite(3, LOW);
  Serial.println("Coolant pump off.");
  Serial.println("Vacuum system off.");
  vacSysRun = 0;
}

void indicateNeedle(String zone) {
  if (zone == "fault") {
    analogWrite(6, 0);
  } else if (zone == "pressure") {
    int indc = (log10(pressureBar)*(RangeMax-RangeMin)/(-2))+RangeMin; //ar-
bitrary calibration parameters, this has to do with the low pass filter & the
resistance of the indicator
    analogWrite(6, indc);
  } else if (zone == "ready") {
    analogWrite(6, 255);
  } else {
    analogWrite(6, 0);
  }
}
```

```
int measureTankPressure() {
  pressInt = analogRead(14);  // read the input pin
  float Vout = float(pressInt) / 1024 * 5; //1024 bit ADC, gives readings be-
tween 1-1024, convert that to voltage, the ADC works over 0-5V
  // Invert and adjust the pressure range
  pressureBar = (Vout-0.5)*(Pmax/(VmaxComp-VminComp));//calibration from
datasheet
  return;
}
```

Figure C.2: Arduino microcontroller code